Nucleic Acids Research, 2026, **54**, gkag832
https://doi.org/10.1093/nar/gkag832
RNA and RNA-protein complexes

hY3 RNA binds and inhibits ribosomes and modulates the starvation-induced integrated stress response

Valentina Pecoraro[1,2], EunBin Kong[1], Puneet Sharma[3], Yulia Gonskikh[1,2,4], Marek Żywicki[5], Fabian Nagelreiter[6], Markus Schosserer[6,7], Katrin Freiburghaus[8,9], Jean-Marc Nuoffer[8], Johannes Grillari[6,10], Norbert Polacek[1,*]

[1]Department of Chemistry, Biochemistry and Pharmaceutical Sciences, University of Bern, Bern 3012, Switzerland
[2]Graduate School for Cellular and Biomedical Sciences, University of Bern, Bern 3012, Switzerland
[3]Institute of Biochemistry, ETH Zürich, Zürich 8093, Switzerland
[4]Present address: Department of Biological Sciences and Pathobiology, University of Veterinary Medicine Vienna, Vienna 1210, Austria
[5]Department of Computational Biology, Institute of Molecular Biology and Biotechnology, Adam Mickiewicz University, Poznań 61-614, Poland
[6]Institute of Molecular Biotechnology, BOKU University, 1190 Vienna, Austria
[7]Institute of Medical Genetics, Center for Pathobiochemistry and Genetics, Medical University of Vienna, Vienna 1090, Austria
[8]University Institute of Clinical Chemistry, Inselspital, Bern University Hospital, University of Bern, Bern 3010, Switzerland
[9]Graduate School for Health Sciences, University of Bern, Bern 3012, Switzerland
[10]Ludwig Boltzmann Institute for Traumatology, The Research Center in Cooperation with AUVA, 1200 Vienna, Austria

*To whom correspondence should be addressed. Email: norbert.polacek@unibe.ch

Abstract

Cells adapt to metabolic stress by orchestrating gene expression to mitigate cellular damage, sustain homeostasis, and promote survival. Within this framework, translational control provides a rapid and efficient layer of regulation. Non-coding RNAs have recently emerged as effective modulators of translation, partly by targeting the ribosome. The contribution of ribosome-associated non-coding RNAs (rancRNAs) to translation regulation, however, remains largely unexplored in human cells. Here, we identified the human Y3 (hY3) RNA as a rancRNA that inhibits protein synthesis and attenuates cellular metabolism. hY3 function was particularly critical under nutrient deprivation, where it promoted adaptive stress responses. In this context, depletion of hY3 disrupted the delicate balance between survival and apoptosis by reducing the expression of pro-survival factors and impairing the activation of the integrated stress response (ISR). Loss of hY3 reduced starvation-dependent phosphorylation of eukaryotic translation initiation factor 2α, thereby attenuating ISR signalling, which results in non-physiologically elevated global translation rates during nutrient deprivation. Together, our findings establish hY3 as a ribosome-bound regulator of translation and stress responses, positioning it as a determinant of cell fate under metabolic stress.

Graphical abstract

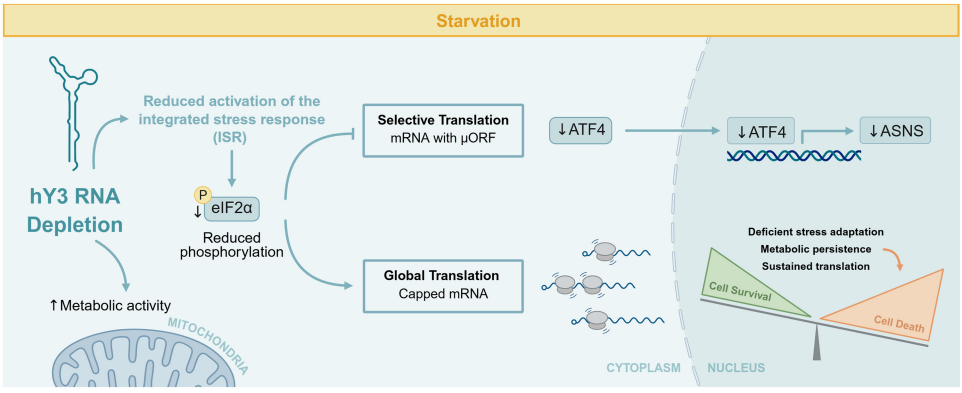

Introduction

Cutting-edge technologies are beginning to spotlight the "dark matter" of genomes, uncovering various types of non-coding RNA (ncRNA) that are essential for orchestrating intricate cellular processes. A subset of these ribo-regulators has been found to target directly the ribosome, the ribozyme

Received: October 19, 2025. **Revised:** June 29, 2026. **Accepted:** July 22, 2026

at the core of the protein synthesis process [1, 2]. These so-called ribosome-associated non-coding RNAs (rancRNAs) have recently emerged on the scene of regulatory ncRNA research as efficient contributors to translation control [1, 2]. They represent a widely heterogeneous group of regulatory RNA molecules, showing diversity in their chromosomal origin, length, and function. Echoing the David versus Goliath paradigm, rancRNAs, despite consisting sometimes of only a few dozen nucleotides, can effectively take control over the cell's giant protein machinery. The association of specific rancRNAs with the ribosome has been experimentally confirmed in various organisms spanning all three domains of life, in particular in the context of cellular stress responses [1]. In most cases, rancRNAs inhibit global translation, but also stimulation of protein biosynthesis has been described [3–6]. When confronted with challenging environmental conditions, such as nutrient deprivation, cells can initiate a protective response to mitigate stress and promote cell survival [7]. In these premises, the regulation of translation during stress is of utmost importance, given that protein synthesis is a highly energy-demanding process that consumes the majority of cellular energy resources [8]. Consequently, the reduction in global protein synthesis allows cells to reallocate the saved energy and resources effectively into cellular maintenance and repair, thereby facilitating the adaptation to adverse environments and the restoration of cellular homeostasis.

One of the key adaptive mechanisms that mammalian cells employ to regulate translation under metabolic stress, alongside the mTOR signaling pathway, is the integrated stress response (ISR) [9]. This adaptive response is initiated by eukaryotic translation initiation factor 2α (eIF2α) kinases, including HRI, PKR, general control nonderepressible 2 (GCN2), and PERK. They sense different stress signals and catalyze the phosphorylation of the alpha subunit of eIF2α at serine 51 [9]. The phosphorylation of eIF2α allows for selective protein synthesis that prioritizes stress-responsive proteins while downregulating general messenger RNA (mRNA) translation [10].

During starvation, the GCN2 kinase phosphorylates eIF2α, which leads to a global downregulation of cap-dependent translation while concomitantly promoting the selective translation of specific mRNAs, including the activating transcription factor 4 (ATF4). ATF4 acts as a master transcriptional regulator of metabolic genes that enable cellular adaptation to stress [10]. One prominent ATF4 target involved in amino acid metabolism is asparagine synthetase (ASNS), which plays a crucial role in maintaining amino acid homeostasis under nutrient shortage conditions [11]. Thus, gene expression reprogramming driven by the ISR is essential for cell survival during metabolic stress. Impaired ISR activation can have detrimental consequences, including reduced expression of stress-responsive genes, disrupted amino acid transport, and diminished resistance to oxidative stress. Ultimately, cells that fail to mount an adequate adaptive response are inevitably destined to programmed cell death [12, 13].

In this study, we identified the human Y3 (hY3) RNA as a novel rancRNA. hY3 is part of the abundant and highly conserved class of ncRNAs, known as Y RNAs [14]. The human genome encodes four Y RNA paralogs, hY1, hY3, hY4, and hY5, which range from 84 to 113 nt in length. They are transcribed by the RNA Polymerase III and are found in both the nucleus and the cytoplasm [15]. It has previously been reported that these ncRNAs are implicated in various cellular processes, including the initiation of DNA replication, RNA quality control, ribonucleoprotein (RNP) assembly, and cellular stress responses [16]. Moreover, the cleavage of Y RNAs performed through the caspase-3 dependent pathway, results in the formation of Y RNA-derived fragments (YsRNAs), which are involved in apoptosis, DNA repair, and promotion of inflammation [17, 18].

Y RNAs are characterized by a conserved hairpin-shaped structure, featuring resembling stem regions and subtype-specific central loop sequences [19]. The loop region serves as a binding site for various RNA-binding proteins (RBPs), many of which regulate transcription and translation [20]. In particular, hY3 has been reported to bind translational regulatory proteins such as the neuron-specific HuD and the ubiquitously expressed HuR [21, 22]. Beyond their intracellular functions, Y RNAs can also contribute to intercellular communication via extracellular vesicles [20]. Indeed, Y RNAs are abundantly present in body fluids and have been proposed as potential biomarkers in cancer, cardiovascular diseases, neurodegenerative pathologies, and immune-related diseases [22–24]. However, while their expression and localization have been extensively studied, the distinct molecular functions of individual Y RNAs remain poorly understood.

Here, we explored the role of hY3 in the regulation of translation and metabolism, and its contribution to cellular susceptibility under nutrient deprivation in primary human dermal fibroblasts (HDFs) and in immortalized cancer cells. Our findings revealed that hY3 binds to ribosomes and polysomes and interferes with the proper activation of ISR, thereby playing a decisive role in determining how cells cope with metabolic stress and regulate apoptosis susceptibility.

Materials and methods

Characteristics of human dermal fibroblasts from two donors

Primary HDF cell lines HDF85 and HDF161 were obtained from healthy donors through Evercyte GmbH (Vienna, Austria). HDF85 cells were derived from a 49-year-old female donor, and HDF161 cells from a 65-year-old female donor, both originating from abdominoplasty tissue. Cells were cultured in Dulbecco's modified Eagle's medium (DMEM)/Ham's F-12 1:1 medium (Biochrom, Cat#FG4815, 500 ml) supplemented with 56 ml fetal bovine serum (FBS) (Sigma–Aldrich, Cat#F7524), and 10 ml of 200 mM L-glutamine (Sigma–Aldrich, Cat#G7513). Cultures were maintained at 37°C in a humidified incubator with 7% CO_2. For induction of stress-induced premature senescence (SIPS), population doubling (PD) 13 was used for HDF85 and PD15 for HDF161. All procedures involving primary human cell lines were conducted in accordance with approved ethical protocols.

Human dermal fibroblasts culture

Primary HDFs from two healthy donors (HDF85 and HDF161, Evercyte GmbH Vienna, Austria) were kindly provided by the group of Johannes Grillari, University of Natural Resources and Life Sciences, Vienna, Austria. Cells were routinely cultured in DMEM/Ham's F-12 1:1 medium (Biochrom, Cat#FG4815, 500 ml) supplemented with 56 ml FBS (Sigma–Aldrich, Cat#F7524) and 10 ml of 200 mM L-glutamine (Sigma–Aldrich, Cat#G7513) at 37°C in a humified

incubator with 7% CO_2 and tested for mycoplasma in regular intervals. Cell counting was performed with the automated cell counter Luna-II™ (Logos Biosystems). Proliferating HDFs were passed twice a week in a ratio of 1:2 to 1:3 and detached with trypsin-ethylenediaminetetraacetic acid (EDTA) (0.05% Trypsin-EDTA, phenol red, Gibco™, Thermo Fisher Scientific, Cat#25300062) at 37°C for 5 min. For both quiescent and senescent conditions, HDFs were seeded at a density of 3500 cells/cm^2 1 day prior to treatment and allowed to adhere overnight. Quiescence was induced by allowing the cells to reach confluency and undergo contact inhibition, with media changes performed once per week. In parallel, senescence was induced in separate HDF cultures by treating cells with doxorubicin.

Stress-induced premature senescence by doxorubicin

For the induction of premature senescence, HDFs were treated twice with freshly prepared DMEM medium containing 200 nM doxorubicin (Sigma–Aldrich, Cat#D1515-10MG; 5 mM stock solution in H_2O stored at −20°C). One day after seeding, the culture medium was replaced with doxorubicin-containing medium, and cells were incubated at 37°C and 7% CO_2 for 4 days. The treatment was then repeated by replacing the medium with freshly prepared doxorubicin-supplemented DMEM, followed by an additional 3 days of incubation. After the second treatment, the doxorubicin-containing medium was removed, and cells were maintained in regular culture medium for 3 weeks, with media changes once per week, to allow recovery and stabilization of the senescent phenotype. Premature senescence was confirmed by senescence-associated β-galactosidase staining following standard protocols, as well as by morphological assessment under light microscopy [25, 26]. Images were captured using a DFC360 FX monochrome camera (Leica Microsystrems) mounted on a DMI6000B microscope (Leica Microsystems).

For complementary DNA (cDNA) library generation, HDFs under proliferating, quiescent, and senescent conditions were prepared by the group of Johannes Grillari and subsequently sent to our lab for further processing and analysis. For northern blot (NB) experiments, primary HDFs were cultured under the same conditions by our group, following the protocols established by the Grillari lab.

Generation of HDF cDNA libraries

For the generation of cDNA libraries, primary HDFs cultured under proliferating, quiescent, and doxorubicin-induced premature senescence conditions were kindly provided by the group of Johannes Grillari. Two biological replicates from donors HDF85 and HDF161 were processed, each in two technical replicates. Cell pellets were resuspended in resuspension buffer containing 30 mM HEPES/KOH (pH 7.6), 150 mM KOAc, 3.9 mM $MgOAc_2$, 4 mM dithiothreitol (DTT), protease inhibitor cocktail (cOmplete™ ULTRA Tablets, Mini, EDTA-free, EASYpack, Roche, Cat#05892791001), RNasin® Ribonuclease Inhibitor (Promega, Cat#N2611). One-tenth of each cell suspension was used for total RNA extraction with TRI Reagent® (Zymo Research, Cat#R2050-1-200) following the manufacturer's instructions.

The remaining cells in suspension were opened by repeated passage through a 25-gauge needle attached to a 1-ml syringe. Cell debris was removed by centrifugation at 20 000 × *g* at 4°C for 15 min. To enrich rancRNA, cDNA libraries were generated from small RNAs that copurified with the crude ribosomal pellet fraction obtained after centrifugation at 200 000 × *g*. For ribosome pellet isolation, the cell lysate was layered onto a 0.5 ml pre-cooled 1.1 M sucrose cushion prepared in 30 mM HEPES-KOH (pH 7.6), 150 mM KOAc, 3.9 mM $MgOAc_2$, 4 mM DTT, and 1 mM PMSF. The ultracentrifugation was performed at 200 000 × *g* for 1.5 h at 4°C using an fixed-angle rotor S140AT in a Sorvall M120 + mini ultracentrifuge (Thermo Fisher Scientific). RNA was extracted from the resulting ribosome pellet using TRI Reagent® (Zymo Research, Cat#R2050-1-200) according to manufacturer's protocol.

Both total RNA and RNA derived from ribosome pellet were size-fractionated by denaturing polyacrylamide gel (8% acrylamide M-Bis, 7 M Urea, 1× TBE). RNAs corresponding to the size range between 18 and 300 nt were excised from the gel, eluted overnight in 0.3 M NaOAc (pH 5.5) with 1 mM EDTA, and precipitated in ethanol with 1 µl GlycoBlue™ Coprecipitant (Invitrogen™, Cat#AM9516). RNA was pelleted by centrifugation at 10 000 × *g* for 2 h at 4°C. To remove cyclic 2′,3′-phosphates at the 3′ end, RNA was treated with T4 polynucleotide kinase (PNK, 10 U/µl, Thermo Fisher Scientific, Cat#EK0032) in a 30 µl reaction containing 1× T4 PNK Reaction Buffer A (Thermo Fisher Scientific, Cat#EK0032), 0.167 mM ATP (Adenosine 5′-triphosphate Sigma–Aldrich, Cat#A8937), 1 µl RiboLock RNase inhibitor (40 U/µl, Thermo Fisher Scientific Cat#EO0382), and 1 µl T4 PNK (10 U/µl Thermo Fisher Scientific, Cat#EK0032), following the protocol described by Honda *et al*. 2016 [27]. The reaction was incubated in a water bath at 37°C for 40 min and subsequently purified using phenol/chloroform/isoamyl alcohol (ROTI®Aqua-P/C/I, Carl Roth, Cat#X985.2) according to the manufacturer's protocol. The quantity and quality of the purified total RNA and the RNA derived from the ribosome pellet were assessed using a Thermo Fisher Scientific Qubit 4.0 fluorometer with the Qubit RNA HS Assay Kit (Thermo Fisher Scientific, Cat#Q32855) and an Advanced Analytical Fragment Analyzer System using a Fragment Analyzer RNA Kit (Agilent, Cat#DNF-471), respectively. Total RNA-Seq libraries were generated using a SMARTer Stranded Total RNA-Seq Kit v2 – Pico Input Mammalian Kit (Takara, Cat#634 413) following the SMARTer Stranded Total RNA-Seq Kit v2 - Pico Input Mammalian User Manual (Takara, Cat#022 025). The cDNA libraries were equimolar pooled and sequenced 50 bp paired-end using a shared illumina NovaSeq 6000 SP Reagent Kit v1 (100 cycles, illumina, Cat#20 027 464).

Analysis of HDF rancRNA sequencing data

Raw sequencing reads have been subjected to adapter trimming using cutadapt software v2.8 [28]. Trimmed reads have been aligned to human reference genome GRCh38 and quantified according to Gencode v28 genome annotation using STAR (v2.7.1a) [29]. Differential expression analysis was performed using DESeq2 package [30].

HeLa cell culture and treatments

HeLa cells (ATCC®, CCL-2™) were cultured in RPMI 1640 medium (Gibco™, Thermo Fisher Scientific, Cat#31870025) supplemented with 10% FBS (Gibco™, Thermo Fisher Scientific, Cat#A5669801), 2 mM L-glutamine, 100 units/ml

penicillin, 100 µg/ml streptomycin (Penicillin-Streptomycin-Glutamine 100×, Gibco™, Thermo Fisher Scientific, Cat#10378016) at 37°C and 5% CO_2. For passaging, cells were washed with phosphate buffered saline (PBS) and detached with trypsin-EDTA (0.05% Trypsin-EDTA, phenol red, Gibco™, Thermo Fisher Scientific, Cat#25300062).

During lipofectamine-mediated transfection, cells were grown in RPMI 1640 medium supplemented with 10% FBS and 2 mM L-glutamine (200 mM, Gibco™, Thermo Fisher Scientific, Cat#25030081), without the addition of antibiotics.

To induce starvation stress, cells were washed twice with PBS and exposed to a low glucose DMEM medium lacking amino acids and serum (DMEM, w: 1.0 g/l Glucose, w/o: L-Glutamine, w/o: Amino acids, w: Sodium pyruvate, w: 3.7 g/l $NaHCO_3$, PAN-Biotech, Cat#P0401507), with exposure time varying from 20 min to 4 h.

Northern blot analysis

RNA extraction was performed either by TRI Reagent® (Zymo Research, Cat#R2050-1-200) or by PCI (ROTI®Aqua-P/C/I, Carl Roth, Cat#X985.2) according to manufacturer's instructions. For NB analysis, 10–20 µg RNA were separated on an 8% denaturing polyacrylamide gel (Acrylamide M-Bis solution 30% 29/1, Gerbu, Cat#1108, 7M Urea, 1× TBE buffer) and transferred to a nylon membrane (Hybond™-N + Positively charged Nylon Transfer Membrane, Cytiva, Cat#RPN203B) at 400 mA for 45 min using a semidry blotting system (V20-SDB, Scie-Plas). After immobilizing RNA using a UV cross-linker (0.120 J/cm^2, BLX-254, Vilber Lourmat) membranes were prehybridized for 30 min in hybridization buffer [1 M sodium phosphate buffer, pH 6.2, 7% sodium dodecyl sulfate (SDS)]. DNA oligonucleotides complementary to the RNA of interest were end-labeled with [γ-32P]-ATP (Hartmann Analytic, Cat#SCP-501) and T4 PNK (Thermo Fisher Scientific, Cat#EK0032). Hybridization was carried out overnight at 42°C. Membranes were then washed as previously described [31]. Signals were detected by exposing membranes to phosphor imaging screens, scanned with a Typhoon phosphor imager (GE Typhoon FLA 9000, GE Healthcare), and quantified using ImageQuant TL-11 (Cytiva).

Oligonucleotide probes used for northern blot analysis

hY1: 5′-AAAGAGTAGAACAAGGAGTTCG-3′
hY3: 5′-GGCTAGTCAAGTGAAGCAGTGGGAG-3′
hY4: 5′-TTGTATACCAACTTTA-3′
hY5: 5′-GGGGAGACAATGTTAA-3′

RT-qPCR analysis

RNA from HDF85 ribosome-enriched pellet was extracted using ROTI®Aqua-P/C/I (Carl Roth, Cat#X985.2). Total RNA from HeLa cells under normal conditions and after 20 min of starvation was isolated using the Direct-zol™ RNA MiniPrep Kit (Zymo Research, Cat#R2050). RNA from ribosome pulldown experiments in HeLa cells was purified using RNA Clean & Concentrator™-5 Kit (Zymo Research, Cat#R1015). RNA concentrations were measured using a NanoDrop spectrophotometer.

Reverse transcription of 200–300 ng RNA was performed with SuperScript™ IV Reverse Transcriptase (Invitrogen™, Cat#18090050), following manufacturer's instructions, with Random Hexamer Primer (Thermo Fisher Scientific, Cat#SO142). qPCR was performed using the GoTaq® qPCR Master Mix (Promega, Cat#A6002) on a Rotor-Gene Q system (QIAGEN), with 3–4 technical replicates for each experiment. Gene-specific primers were synthesized by Microsynth.

Primers used for RT-qPCR analysis

hY1 Forward: 5′-GGCTGGTCCGAAGGTAGTGA-3′ [32]
hY1 Reverse: 5′-GCAGTAGTGAGAAGGGGGGA-3′ [32]
hY3 Forward: 5′-GGCTGGTCCGAGTGCAGTGG-3′ [32]
hY3 Reverse: 5′-GAAGCAGTGGGAGTGGAGAA-3′ [32]
hY4 Forward: 5′-GGCTGGTCCGATGGTAGTGG-3′ [32]
hY4 Reverse: 5′-TTAGCAGTGGGGGGTTGTAT-3′ [32]
hY5 Forward: 5′-AGTTGGTCCGAGTGTTGTGG-3′ [32]
hY5 Reverse: 5′-AACAGCAAGCTAGTCAAGCG-3′ [32]
18S rRNA Forward: 5′-GAGAAACGGCTACCACATCCA-3′ [33]
18S rRNA Reverse: 5′-CTCCAATGGATCCTCGTTAA AGG-3′ [33]
GAPDH Forward: 5′-TCAAGGCTGAGAACGGGAAG-3′ [34]
GAPDH Reverse: 5′-CGCCCCACTTGATTTTGGAG-3′ [34]
SCD Forward: 5′-CTCTGCTACACTTGGGAGCC-3′ [35]
SCD Reverse: 5′-GAGCTCCTGCTGTTATGCCC-3′ [35]
CS Forward: 5′-GGACAATTTTCCAACCAATCTGC-3′ [36]
CS Reverse: 5′- AGTCAATGGCTCCGATACTGC-3′ [36]
KRT17 Forward: 5′-GGTGGGTGGTGAGATCAATGT-3′ [37]
KRT17 Reverse: 5′-CGCGGTTCAGTTCCTCTGTC-3′ [37]
Bcl-xL Forward: 5′- CGGTACCGGCGGGCATTCAG-3′ [38]
Bcl-xL Reverse: 5′- CGGCTCTCGGCTGCTGCATT-3′ [38]
CDK6 Forward: 5′-CCAGGCAGGCTTTTCATTCA-3′ [39]
CDK6 Reverse: 5′-AGGTCCTGGAAGTATGGGTG-3′ [39]
ASNS Forward: 5′-TGGCTGCCTTTTATCAGGGG-3′ [40]
ASNS Reverse: 5′-TCTGCCACCTTTCTAGCAGC-3′ [40]
ATF4 Forward: 5′- GGAGATAGGAAGCCAGACTACA -3′ [41]
ATF4 Reverse: 5′- GGCTCATACAGATGCCACTATC-3′ [41]

Polysome profiling

Prior to cell harvest, cells were treated with freshly prepared cycloheximide (CHX) (100 µg/ml, Carl Roth, Cat#8682.3) for 10 min. Cells were then washed with ice-cold PBS and lysed in buffer consisting of 30 mM HEPES/KOH (pH 7.6), 150 mM KOAc, 3.9 mM $MgOAc_2$, 4 mM DTT, 1% Triton™ X-100 (Sigma–Aldrich, Cat#T8787), protease inhibitor cocktail (cOmplete™ ULTRA Tablets, Mini, EDTA-free, EASYpack, Roche, Cat#05892791001), RNasin® Ribonuclease Inhibitor (Promega, Cat#N2611), and 100 ng/ml CHX (Carl Roth, Cat#8682.3). To ensure complete cell lysis, the suspension was passed eight times through a 25G needle and centrifuged at 500 × *g* for 2 min at 4°C (Eppendorf Centrifuge 5804R, rotor F45-30-1). The supernatant was transferred to

a new tube and centrifuged at 10 000 × *g* for 5 min at 4°C. The clarified lysate was collected into a fresh tube. For EDTA treatment, HeLa cell lysate was incubated with 80 mM EDTA (Gerbu, Cat#1034) for 30 min on ice.

Cell lysates containing 10–20 A_{260} units were applied to linear 10%–50% (w/v) sucrose gradients prepared in gradient buffer (30 mM HEPES/KOH, pH 7.6, 150 mM Kac, 5 mM $MgAc_2$, 4 mM DTT, 1 mM PMSF, 100 μg/ml CHX). For dissociation experiments, lysates were treated with EDTA and layered onto gradients prepared in dissociation buffer (30 mM HEPES/KOH, pH 7.6, 150 mM Kac, 1 mM $MgAc_2$, 4 mM DTT, 1 mM PMSF). Gradients were centrifuged using a SW-41 swing-out rotor (Beckman) at 39 000 rpm for 2 h 45 min at 4°C. Subsequently, gradients were fractionated with a piston gradient fractionator (Biocomp) and monitored by UV absorbance at 260 nm. Fractions corresponding to free RNA, 40S, 60S, 80S, and polysomes were collected. RNA from each fraction was extracted with ROTI®Aqua-P/C/I (Carl Roth, Cat#X985.2) and precipitated using isopropanol in the presence of 1 μl GlycoBlue™ Coprecipitant (Invitrogen™, Cat#AM9516).

For purification of the 40S and 60S ribosomal subunits, cell lysates were incubated with 50 mM EDTA for 30 min on ice with intermittent vortexing, then applied to linear 10%–40% (w/v) sucrose gradients prepared in dissociation buffer. Gradients were centrifuged for 6 h at 39 000 rpm, 4°C, and fractions containing 40S and 60S subunits were identified by polysome profiling and pooled.

To purify 80S ribosomes, cell lysates were supplemented with 100 μg/ml puromycin (Sigma–Aldrich, Cat#P7255) and incubated at 37°C with shaking at 500 rpm for 15 min. Lysates were layered onto linear 10%–40% (w/v) sucrose gradients prepared in gradient buffer and centrifuged for 2.5 h at 39 000 rpm, 4°C. Fractions containing 80S ribosomes were identified by polysome profiling and pooled.

For ribosome and subunit pelleting, pooled fractions containing 40S, 60S subunits, or 80S ribosomes were diluted in 10% sucrose solution and subjected to overnight centrifugation for 16 h at 39 000 rpm, 4°C. The resulting pellets were resuspended for downstream analysis.

In vitro transcription

DNA templates for hY3, hY3 mutant, Scrambled, and hY1 were generated by PCR. For template assembly, long primers containing the T7 RNA polymerase promoter sequence were first annealed and extended. The resulting products were then amplified PCR using shorter primers.

hY3 Primer Extension Forward 5′-3′:
GGATCCTAATACGACTCACTATAGGCTGGTCCGAGTGCAGTGGTGTTTACAACTAATTGATCACAACCAGTT

hY3 Primer Extension Reverse 5′-3′: AAAAGGCTAGTCAAGTGAAGCAGTGGGAGTGGAGAAGGAACAAAGAAATCTGTAACTGGTTGTGATCAATTAG

hY3 Primer Amplification Forward 5′-3′: GGGATCCTAATACGACTCACTATA

hY3 Primer Amplification Reverse 5′-3′: AAAAGGCTAGTCAAGTGAAGC

hY3 Δ54–70 Primer Extension Forward 5′-3′:
GGATCCTAATACGACTCACTATAGGCTGGTCCGAGTGCAGTGGTGTTTACAACTAATTGATCACAACCAGTT

hY3 Δ54–70 Primer Extension Reverse 5′-3′:
AAAAGGCTAGTCAAGTGAAGCAGTGGGAGTGGCTGTAACTGGTTGTGATCAATTAG

hY3 Δ54–70 Primer Amplification Forward 5′-3′: GGGATCCTAATACGACTCACTATA

hY3 Δ54–70 Primer Amplification Reverse 5′-3′: AAAAGGCTAGTCAAGTGAAGC

Scrambled Primer Extension Forward 5′-3′: GGATCCTAATACGACTCACTATAGACGTTCTATTAACTTGCTCTATCTATTGTCTTAGTTCCATATATCATGT

Scrambled Primer Extension Reverse 5′-3′: GACGGCTCGTAACGAACTTGGCAGGATCGAGTTGCCGAGTATCAGAGCGCAGACATGATATATGGAACTAAGA

Scrambled Primer Amplification Forward 5′-3′: GGGATCCTAATACGACTCACTATA

Scrambled Primer Amplification Reverse 5′-3′: GACGGCTCGTAACGAACTTG

Scrambled 2 Primer Extension Forward 5′-3′: GGATCCTAATACGACTCACTATAGTTCCGTGGTATTAATCGTCCTACTCTCCTGTCGTAACTAAGTGAGTAC

Scrambled 2 Primer Extension Reverse 5′-3′: TAGGAAGGTGGACGAACCTAGCGATATCGATTGATTACAGACAAGGTAGCAGAGTACTCACTTAGTTACGAC

Scrambled 2 Primer Amplification Forward 5′-3′: GGGATCCTAATACGACTCACTATA

Scrambled 2 Primer Amplification Reverse 5′-3′: TAGGAAGGTGGACGAACCTAG

PCR products were purified with the Wizard® SV Gel and PCR Clean-Up System (Promega, Cat#A9281). *In vitro* transcription reactions were performed under the following standard conditions: 40 mM Tris–HCl (pH 7.5), 40 mM DTT, 2 mM spermidine, 3.75 mM of each NTP, 20 mM $MgCl_2$, T7 RNA Polymerase (Thermo Fisher Scientific, Cat#EP0111), RNasin® Ribonuclease Inhibitor (Promega, Cat#N2611), and 10 μg DNA template/ml [42]. For crosslinking experiments, 4-Thio-UTP (Jena Bioscience, Cat#NU-1156) was included at an 80% substitution rate. Transcription reactions were incubated in a water bath at 37°C for 6–7 h.

Transcribed RNAs were purified with ROTI®Aqua-P/C/I (Carl Roth, Cat#X985.2) and precipitated in isopropanol using 1 μl GlycoBlue™ Coprecipitant (Invitrogen™, Cat#AM9516). Further purification was performed by size-exclusion chromatography using Sephadex® G-25 (Sigma–Aldrich, Cat#G2580) in 0.3 M NaOAc.

For filter binding and crosslinking assays, transcribed RNA was denatured at 95°C for 2 min, cooled, and dephosphorylated with Quick CIP (New England Biolabs, Cat#M0525) at 37°C for 30 min. RNA was then phenol-chloroform extracted, precipitated in isopropanol with 1 μl GlycoBlue™ Coprecipitant, and 5′ end-labeled with T4 Polynucleotide Kinase (Thermo Fisher Scientific, Cat#EK0032) and [γ-32P]-ATP (Hartmann Analytic, Cat#SCP-501). Labeled RNA was purified with illustra MicroSpin™ G-25 Columns (Cytiva, Cat#27-5325-01) according to the manufacturer's instructions prior to use.

In vitro binding studies

Binding studies of hY3 and hY3 Δ54–70 with ribosomes were performed using a dot blot-filtering device. A scrambled sequence of hY3 served as a negative control for background binding. For each experiment, 3 pmol of purified HeLa ribosomal particles (80S, 60S, or 40S) were incubated with 3 pmol of 5′[32P]-end-labeled *in vitro*-transcribed

RNA in a final volume of 25 µl binding buffer (30 mM HEPES-KOH, pH 7.6, 150 mM KOAc, 3.9 mM $MgOAc_2$, 4 mM DTT). Following 30 min incubation at 37°C, reactions were diluted with 175 µl ice-cold binding buffer and filtered through pre-equilibrated nitrocellulose membranes (Amersham™ Protran™ Premium 0.45 µm NC Nitrocellulose blotting membrane, Cytiva, Cat#10600003) using a vacuum filtration device. Membranes were washed twice with 200 µl ice-cold binding buffer, dried, and exposed to phosphor imaging screens. Radioactive signals were acquired using a Typhoon FLA 9000 phosphor imager (GE Healthcare) and quantified with ImageQuant TL-11 software (Cytiva).

Crosslinking of 4-thio-U-hY3 to HeLa ribosomes

For crosslinking experiments, 4 pmol of 5′[32P]-end-labeled *in vitro*-transcribed hY3 RNA substituted with 80% 4-thiouridine (4-thioU) were incubated with 4 pmol of purified HeLa ribosomal particles (80S, 60S, or 40S) in a final volume of 18 µl binding buffer (30 mM HEPES-KOH, pH 7.6, 150 mM KOAc, 3.9 mM $MgOAc_2$, 4 mM DTT). Two scrambled sequences served as negative controls for background binding (Scrambled and Scrambled 2; Scrambled 2 was used exclusively in crosslinking experiments). Following 30 min incubation at 37°C, samples were placed on ice and UV-crosslinked at 365 nm for 15 min. Control samples were incubated on ice without UV exposure. One control reaction was subsequently treated with Protease K for 15 min at 37°C after crosslinking. All samples were supplemented with 6 µl of 4× Laemmli buffer, heated at 95°C for 5 min, and resolved on 7% SDS–polyacrylamide gel electrophoresis (PAGE) gels. Gels were dried onto Whatman® gel blotting paper (Grade GB003, Sigma–Aldrich, Cat#WHA10426892) and exposed to phosphor imaging screens. Radioactive signals were acquired using a Typhoon FLA 9000 phosphor imager (GE Healthcare).

In vitro translation in HeLa cell extracts

In vitro translation systems using crude HeLa cell lysates were prepared according to a previously described protocol [43]. HeLa cells were cultured in 150 cm^2 plates and harvested at 80%–90% confluency using trypsin-EDTA (0.05% Trypsin-EDTA 1×, Gibco™, Thermo Fisher Scientific, Cat#25 300 062) at 37°C for 5 min. Cell pellets were resuspended in 400 µl lysis buffer [30 mM HEPES/KOH, pH 7.6, 150 mM KOAc, 3.9 mM $MgOAc_2$, 4 mM DTT, 1% TritonTM X-100 (Sigma–Aldrich, Cat#T8787), protease inhibitor cocktail (cOmplete™ ULTRA Tablets, Mini, EDTA-free, EASYpack, Roche, Cat#05892791001), and RNasin® Ribonuclease Inhibitor (Promega, Cat#N2611)]. To ensure complete cell lysis, cell suspensions were passed 10 times through a 25-gauge needle attached to a 1-ml syringe. After removal of cell debris by centrifugation at 20 000 × *g* for 15 min at 4°C, lysates were diluted to 10–15 mg/ml with resuspension buffer containing 30 mM HEPES/KOH (pH 7.6), 150 mM KOAc, 3.9 mM $MgOAc_2$, 4 mM DTT, protease inhibitor cocktail (cOmplete™ ULTRA Tablets, Mini, EDTA-free, EASYpack, Roche, Cat#05892791001), and RNasin® Ribonuclease Inhibitor (Promega, Cat#N2611).

Translation reactions were prepared by combining 6 µl cell lysate with water to a final volume of 9.9 µl. To study hY3 effect on translation, water was replaced with 100 pmol of *in vitro*-transcribed RNA (hY1, hY3, or Scrambled control). CHX at a final concentration of 7.5 mg/ml was used as a translation inhibition control. After pre-incubation at 37°C for 10 min, 2.1 µl of freshly prepared translation mix was added, consisting of: 1.2 µl 10× translation cocktail [150 mM HEPES/KOH, pH 7.6, 750 mM KOAc, 19.5 mM $MgOAc_2$, 4 mM GTP, 17.5 mM ATP, 500 µM amino acid mixture minus methionine (Promega, Cat#L996B)], 0.17 µl H_2O, 0.08 µl 3 M creatine phosphate, 0.06 µl 20 mg/ml creatine phosphokinase (prepared in water with 40% glycerol), and 0.625 µl ^{35}S-methionine (10 µCi/µl, Hartmann Analytic, Cat#SCIS-103) for a final reaction volume of 12 µl. Translation reactions were incubated at 37°C for 20 min and stopped with 12 µl 2× Laemmli buffer. After boiling samples for 5 min at 95°C, reactions were resolved on 10% SDS-polyacrylamide gels. Gels were stained with Coomassie solution, destained, vacuum-dried at 70°C for 45 min onto Whatman® gel blotting paper (Grade GB003, Sigma–Aldrich, Cat#WHA10426892), and exposed to phosphor imaging screens. Radioactive signals were acquired using a Typhoon FLA 9000 phosphor imager (GE Healthcare) and quantified with ImageQuant TL-11 software (Cytiva).

Metabolic labeling

For metabolic labeling experiments, HeLa cells were grown in 12-well plates. Following siRNA (small interfering RNA) transfection or hY3 overexpression, cells were incubated with fresh 1 ml RPMI 1640 medium (Gibco™, Thermo Fisher Scientific, Cat#31 870 025) supplemented with 1 µl ^{35}S-methionine (10 µCi/µl, Hartmann Analytic, Cat#SCIS-103) for 1 h at 37°C. Cells were then harvested by scraping in 60 µl lysis buffer containing 30 mM HEPES/KOH (pH 7.6), 150 mM KOAc, 3.9 mM $MgOAc_2$, 4 mM DTT, 1% Triton™ X-100 (Sigma–Aldrich, Cat#T8787), protease inhibitor cocktail (cOmplete™ ULTRA Tablets, Mini, EDTA-free, EASYpack, Roche, Cat#05892791001), and RNasin® Ribonuclease Inhibitor (Promega, Cat#N2611), and supplemented with 20 µl 4× Laemmli buffer. After brief sonication on ice, samples were boiled for 5 min at 95°C. A 10 µl aliquot of each reaction was resolved on 10% SDS-polyacrylamide gels. Gels were stained with Coomassie solution, destained, vacuum-dried at 70°C for 45 min onto Whatman® gel blotting paper (Grade GB003, Sigma–Aldrich, Cat#WHA10426892), and exposed to phosphor imaging screens. Radioactive signals were acquired using a Typhoon FLA 9000 phosphor imager (GE Healthcare) and quantified with ImageQuant TL-11 software (Cytiva).

Overexpression of hY3

DNA from HeLa cells was extracted using TRI Reagent® (Zymo Research, Cat#R2050-1-200). After removing the aqueous phase, DNA was precipitated with 100% ethanol and pelleted by centrifugation at 2000 × *g* for 5 min at 4°C. The pellet was resuspended in 0.1 M sodium citrate in 10% ethanol (pH 8.5), incubated for 30 min, and centrifuged at 2000 × *g* for 5 min at 4°C. This washing step was repeated twice. The pellet was then resuspended in 75% ethanol, incubated for 20 min, and centrifuged at 2000 × *g* for 5 min at 4°C. After air-drying the pellet, it was resuspended in 8 mM NaOH and centrifuged at 12 000 × *g* for 10 min at 4°C to remove insoluble material. The pH was adjusted to 8.0 with HEPES, and DNA concentration was measured using a NanoDrop spectrophotometer.

Primers used for amplification of the hY3 sequence from genomic DNA:

Forward: 5′-ACCGTGGGAGTCTTTGATGG-3′
Reverse: 5′-GGAACAGAAAATGCTTTCCCACC-3′

PCR was performed using Phusion® High-Fidelity DNA Polymerase (New England Biolabs, Cat#M0530) according to the manufacturer's protocol with an annealing temperature of 57°C, 5× Phusion GC Buffer, and 250 ng genomic DNA template. PCR products were resolved on 1% low-melting-point agarose gels and purified using the Wizard® SV Gel and PCR Clean-Up System (Promega, Cat#A9281).

For standard cloning of PCR products into pGEM®-T Easy vector systems (Promega, Cat#A1360), A-tailing was performed by adding Taq DNA Polymerase (New England Biolabs, Cat#M0267) and incubating at 72°C for 20 min according to the manufacturer's protocol. Ligations were performed according to the manufacturer's protocol (pGEM®-T Easy Vector System, Promega, Cat#A1360) using 50 ng vector and 5 ng insert, incubated for 1 h at room temperature. XL1-Blue competent cells were incubated with the ligation mixture for 45 min on ice, followed by heat shock at 42°C for 45 s. Samples were incubated on ice for 2 min, diluted with 300 µl LB medium, and incubated at 37°C with shaking for 1 h. Cells were plated on LB-ampicillin selection plates containing IPTG and X-gal and incubated overnight at 37°C.

Successfully transformed colonies were cultured overnight, and plasmid DNA was isolated using the Wizard® Plus SV Minipreps DNA Purification System (Promega, Cat#A1330) before sequencing at Microsynth using SP6 primer. Subsequently, midiprep was performed using the QIAGEN® Plasmid Plus Midi Kit (Qiagen, Cat#12943) following the manufacturer's protocol. Plasmid DNA integrity was verified by agarose gel electrophoresis, and concentration was measured using a NanoDrop spectrophotometer.

For the overexpression of the hY3 deletion mutant Δ54–70, site-directed mutagenesis was performed on a pGEM®-T Easy vector containing the hY3 WT sequence using PCR with the following primers:

Forward: 5′-AGTTACAGCCACTCCCACTGCTTCACT-3′
Reverse: 5′-GGAGTGGCTGTAACTGGTTGTGATC AATTAGT-3′

Following PCR amplification, the parental plasmid DNA was digested with DpnI (New England Biolabs, Cat#R0176S). The PCR product was subsequently purified using the Wizard® SV Gel and PCR Clean-Up System (Promega, Cat#A9281).

For transfection experiments, HeLa cells were seeded at 0.8×10^5 cells per well in 12-well plates 12 h prior to transfection. Plasmid DNA (0.5 µg) was transfected using 1.5 µl Lipofectamine™ 3000 Reagent (InvitrogenTM, Cat#L3000008) in antibiotic-free RPMI 1640 medium (Gibco™, Thermo Fisher Scientific, Cat#31870025) according to the manufacturer's protocol. After 6 h, cells were washed with PBS, and fresh RPMI medium supplemented with antibiotics was added. Cells were used for experiments 24 h post-transfection.

siRNA transfection

HeLa cells were seeded at a density of 0.3×10^5 cells per well in 24-well plates, 0.6×10^5 cells per well in 12-well plates, and 1.5×10^5 cells per well in six-well plates. After 12 h, cells were transfected with siRNA using Lipofectamine™ RNAiMAX Transfection Reagent (Invitrogen™, Cat#13778075) in antibiotic-free RPMI 1640 medium (Gibco™, Thermo Fisher Scientific, Cat#31870025), following manufacturer's instructions. The transfection complexes were prepared in Opti-MEM™ Reduced Serum Medium (Gibco™, Cat#31985062). For each well format, the following amounts were used: 2.5 pmol siRNA and 1.5 µl Lipofectamine in 24-well plates, 5 pmol siRNA and 3 µl Lipofectamine in 12-well plates, and 13 pmol siRNA and 7 µl Lipofectamin in six-well plates. Cells were incubated for 48 h post-transfection before being employed for downstream experiments.

hY1 siRNA: 5′-UGUUCUACUCUUUCCCCCCUU-3′ [44]
hY3 siRNA: 5′-CUAAUUGAUCACAACCAGU-3′ [44]
hY3_2 siRNA: 5′-AUUUCUUUGUUCCUUCUCCAC-3′ [44]
hY3_3 siRNA: 5′-UUUACAACUAAUUGAUCACAA-3′ [44]
Non-targeting negative control siRNA: 5′-AGGUAGUGUAAUCGCCUUG-3′ (Microsynth)

rRNA level analysis

2×10^5 HeLa cells transfected with hY1, hY3, or control siRNA were collected in TRI Reagent® (Zymo Research, Cat#R2050-1-200). Two micrograms Spike-in RNA were added to each sample as an internal control. RNA extraction was performed according to the manufacturer's protocol and precipitated using isopropanol in the presence of 1 µl GlycoBlue™ Coprecipitant (Invitrogen™, Cat#AM9516). Extracted RNA was mixed with RNA Gel Loading Dye 2× (Thermo Fisher Scientific, Cat#R0641) containing ethidium bromide (EtBr). RNA samples were denatured at 70°C for 3 min and loaded onto a 1% denaturing agarose gel. Electrophoresis was performed at 100 V for 1.5 h. EtBr fluorescence of ribosomal RNA (rRNA) bands was normalized to spike-in RNA levels for quantitative analysis.

Cell proliferation and viability assays

HeLa cells were seeded in 24-well plates at 0.3×10^5 cells/well and transfected 12 h later with control, hY1, or hY3 siRNA. An untreated condition served as additional control.

For proliferation assays, cells were harvested and counted at 0 h (time of transfection), 24 h, and 48 h post-transfection. For viability assays, 48 h post-transfection cells were incubated in low-glucose DMEM medium lacking amino acids and serum (DMEM with 1.0 g/l glucose, without L-glutamine, without amino acids, with sodium pyruvate, with 3.7 g/l $NaHCO_3$; PAN-Biotech, Cat#P0401507). Viability was assessed at 0, 1, 2, 3, and 4 h of starvation. Images were acquired with Nikon Mikroskop Eclipse TS2.

For cell counting, cells were detached with 0.05% trypsin-EDTA (Gibco™, Thermo Fisher Scientific, Cat#25300062) at 37°C for 5 min and counted using a LUNA-II™ Automated Cell Counter (Logos Biosystems).

Seahorse XFe96 metabolic flux analysis

Metabolic flux was analyzed using a Seahorse XFe96 analyzer (Agilent Technologies). Oxygen consumption rate (OCR), an indicator of mitochondrial respiration, and extracellular acidification rate (ECAR), a measure of glycolysis, were recorded simultaneously. HeLa cells transfected with hY3, hY3_2, hY3_3, or control siRNA in DMEM/F-12 (Gibco™, Cat#21331046, supplemented with 10% FBS, Gibco™, Cat#A5669801, and 1× Pen-Strep glutamine, Gibco™,

Cat#10378016) were seeded at a density of 20 000 cells/well in a 96-well assay plate 24 h prior to analysis. On the day of the experiment, cells were washed twice with assay medium (DMEM, Merck, Cat#D5030) supplemented with 5.5 mmol/l glucose (Merck, Cat#G7021), 1 mmol/l sodium pyruvate (Merck, Cat#P5240), 5 mmol/l HEPES (Merck, Cat#H0887), 0.2 mmol/l MEM non-essential amino acids (Gibco, Cat#11140035), 0.5 mg/ml penicillin, streptomycin, and glutamine; pH 7.4 (Gibco, Cat#10378016). Following a 1 h incubation at 37°C in a non-humidified, CO_2-free incubator, a mito stress test was performed using Seahorse XFE96 flux paks (Agilent Technologies, Cat#103792-100). OCR and ECAR were measured under basal conditions followed by a sequential injection of oligomycin (1 µmol/l, complex V inhibitor, Merck, Cat#O4876), carbonyl cyanide-p-trifluoromethoxyphenylhydrazone (FCCP) (0.75 µmol/l, uncoupler, Merck, Cat#SML2959), and rotenone (1 µmol/l, complex I inhibitor, Merck, Cat#R8875)/antimycin A (0.5 µmol/l, complex III inhibitor, Merck, Cat#A8674) mix. Optimal concentrations of these metabolic modulators were determined via prior titration. Bioenergetic profiling was conducted on background-corrected OCR and ECAR data as previously described [45]. ORC and ECAR data were normalized to total DNA content (CyQuant, Invitrogen, Cat#C7026). Control cells were analyzed in two biological replicates, and hY3-depleted cells in three biological replicates; all groups included eight technical replicates

MTT assay

HeLa cells were seeded in a 24-well plate at a density of 0.3×10^5 cells/well and transfected with control, hY1, or hY3 siRNA. An untreated condition was included as additional control. Forty-eight hours post-transfection, 250 µl of MTT solution (5 mg/ml in PBS; Invitrogen™, Cat#M6494) were added to each well and incubated at 37°C for 1 h. The MTT solution was then removed, and 300 µl of DMSO (Carl Roth, Cat#7029.1) were added to solubilize the formazan crystals. Absorbance was measured at 570 nm using a Tacan plate reader. To account for differences in cell number, a parallel plate of identically treated cells was used for cell counting with the LUNA-II™ Automated Cell Counter (Logos Biosystems). Relative metabolic activity was calculated by normalizing the MTT absorbance values to the corresponding cell counts for each condition.

Western blot analysis

Cells were harvested in RIPA lysis buffer containing 150 mM NaCl, 50 mM Tris–HCl (pH 8), 0.1% SDS, 0.5% sodium deoxycholate, and 1% NP-40 (IGEPAL® CA-630, Sigma–Aldrich, Cat#56741–50ML-F) supplemented with Protease Inhibitor Cocktail (Roche, Cat#05892791001) and Phosphatase Inhibitor (Thermo Fisher Scientific, Cat#A32957). Lysates were centrifuged at 16 000 × *g* for 10 min at 4°C to remove debris. Protein concentration was determined by the Pierce™ BCA Protein Assay Kit (Thermo Fisher Scientific, Cat#23227).

Between 30 and 50 µg of total protein was resolved by SDS–PAGE, then transferred to Amersham™ Protran™ Premium 0.45 µm NC Nitrocellulose membrane (Cytiva, Cat#10600003). Membranes were blocked with 3% milk in TBST and incubated with primary antibodies diluted in blocking solution: GAPDH (1:2000, Rabbit Anti-GAPDH Monoclonal Antibody, Cell Signaling Technology, Cat#2118; RRID:AB_561053), ATF4 (1:1000, ATF-4 (B-3), Santa Cruz Biotechnology, Cat#sc-390063; RRID:AB_2810998), ASNS (1:1000, ASNS (G-10), Cat#sc-365809; RRID:AB_10843357), eIF2α (1:2500, eIF2 alpha Antibody, Cell Signaling Technology, Cat#9722; RRID:AB_2230924), phospho-eIF2α (p-eIF2α) (1:2500, Phospho-eIF2alpha (Ser51) Antibody, Cell Signaling Technology, Cat#9721; RRID:AB_330951), Bcl-xL (1:1000, Bcl-xL (54H6) Rabbit mAb, Cell Signaling Technology, Cat#2764, RRID:AB_2228008), PARP1 (1:1000, PARP-1 (F-2), Santa Cruz Biotechnology, Cat#sc-8007; RRID:AB_628105), and P62 (1:1000, SQSTM1/p62 (D5L7G) Mouse mAb, Cell Signaling Technology, Cat#88 588; RRID:AB_2800125). HRP-conjugated secondary antibodies (1:2000 dilution in 3% Milk/TBST, Anti-mouse IgG, HRP-linked Antibody, Cell Signaling Technology, Cat#7076; RRID:AB_330924, Anti-rabbit IgG, HRP-linked Antibody, Cell Signaling Technology, Cat#7074; RRID:AB_2099233) were used for detection.

Proteins were visualized using SuperSignal™ West Femto Maximum Sensitivity Substrate (Thermo Fisher Scientific, Cat#34095). Representative blots from three or four independent experiments are shown in the figures. Quantification of band intensities was performed using ImageQuant TL-11 software (Cytiva).

RNA isolation and sequencing of translationally active ribosome-associated RNAs

Translationally active ribosome-associated RNAs were isolated using the AHARIBO RNA System (Immagina Biotechnology, Cat#AHA-RM12). Briefly, 150 000 HeLa cells per well were seeded in six-well plates and cultured in RPMI 1640 medium (Gibco™, Cat#31870025). Cells were transfected with 13 pmol siRNA using 7 µl Lipofectamine™ RNAiMAX (Invitrogen™, Cat#13778075) prepared in Opti-MEM™ Reduced Serum Medium (Gibco™, Cat#31985062); transfections were performed in RPMI 1640 medium without antibiotics. After 48 h, media was removed, and cells were washed twice with PBS.

Cells were incubated for 20 min at 37°C in low glucose DMEM medium lacking amino acids and serum (DMEM, w: 1.0 g/l Glucose; w/o L-Glutamine, w/o Amino acids; w/ Sodium pyruvate; w/ 3.7 g/l NaHCO3; PAN-Biotech, Cat#P0401507) supplemented with 10 µl L-azidohomoalanine (AHA). After addition of 2.6 µl sBlock, cells were incubated for an additional 5 min at 37°C. Cells were placed on ice, washed with cold PBS, and lysed with 45 µl cold lysis buffer, followed by vigorous scraping. Lysates were centrifuged at 20 000 × *g* for 5 min at 4°C. The supernatant was collected, kept on ice for 20 min, and its absorbance measured at 260 nm on a NanoDrop, using lysis buffer for blank subtraction.

Pull-down of active ribosomes was performed by diluting 2 absorbance units (AU) of lysate to 100 µl with freshly prepared Supplemented WB (SWB) Buffer, adding 100 µl of functionalized sBeads, and incubating for 60 min on a slow rotator at 4°C. Beads were washed twice with 700 µl WSS solution and resuspended in 50 µl SWB Buffer. Ribosome-bound RNA was extracted from the bead suspension using the RNA Clean & Concentrator™-5 Kit (Zymo Research, Cat#R1015) and eluted in 15 µl nuclease-free water.

For comparative analysis, HeLa cells grown in complete RPMI 1640 medium or starved in low glucose DMEM (as earlier) for 20 min were collected in 1 ml TRI Reagent® (Zymo Research, Cat#R2050-1-200) and RNA was extracted with the Direct-zol™ RNA MiniPrep Kit (Zymo Research, Cat#R2050), eluted in 50 µl.

All RNA samples underwent rRNA depletion (H/R/M) prior to library preparation. Sequencing libraries were generated using Lexogen's CORALL™ RNA-Seq V2 Library Prep Kit with UDIs. Libraries were sequenced as single-end 100 bp reads (SR100).

Reference genomes and annotations (RNA-seq in HeLa cells)

The reference genome and transcriptome for human (GRCh38; annotation version 113) was obtained from ENSEMBL [46].

Bulk RNA sequencing (RNA-seq in HeLa cells)

Decoy (full genome) aware indexing of transcriptome was done using salmon with the parameter "–kmerLen 31″ [47]. Single-end reads from bulk RNA-seq datasets were processed to remove the Illumina universal adapter (AGATCGGAAGAGCACACGTCTGAACTCCAGTCA) using Cutadapt (v4.4) with the parameters "-q 25 -m 25 –cut 12" [28]. The resulting filtered reads were quantified against the index using Salmon with the parameters "–libType A –gcBias –seqBias –useVBOpt –validateMappings." Subsequent data analysis was performed with custom scripts in R. Data wrangling and visualization were performed using tidyverse package (v2.0.0) [48]. Transcript quantifications were imported using Tximeta [49] and differential expression analysis was conducted using DESeq2 (v1.44) [50].

Differential expression analysis between hY3 siRNA and Control siRNA groups was performed using the python3 gprofiler-official toolkit (v1.0) [51], accessing g:Profiler databases (v2025.01.31). Significantly differentially expressed genes were defined as having absolute log fold change > thresholds mentioned in respective figures and adjusted *P*-value < .05. Volcano plot analysis was conducted using the python package matplotlib (v3.10).

Reference genomes and annotations (RNA-seq in HeLa cells)

To assess biological pathway enrichment using the differential expression results, we used the gprofiler-official Python package incorporating annotations from Reactome, Gene Ontology (GO) Biological Processes, and GO Cellular Components. We utilized genes with ±0.585 $\log_2$-fold change expression and false discovery rate (FDR) < 0.05 applying Benjamini–Hochberg correction for multiple comparisons and assessed the top 10 (for GO) and five upregulated and downregulated pathways, deeming pathways with a *P*-value < .05 as significant.

Preranked gene set enrichment analysis (GSEA) was performed using the GSEApy package with GO:CC_Mitochondrion gene set collection (GO:0 005 739), GO:BP cytoplasmic translation gene set collection (GO:0 002 181) and GP:BP ribosome biogenes gene set collection (GO:0 042 254) and starvation states as input, using the calculated $\log_2$-fold change multiplied by -$\log_{10}$(FDR) as the rank statistic. We further selected the top 20 enriched genes and computed their z-score per replicate to compare hY3 and control siRNA conditions.

Quantification and statistical analylsis

Statistical analyses and the sample sizes for each experiment are specified in the respective figure legends. Data were analyzed and visualized using GraphPad Prism 10.

Results

hY3 associates with the ribosome

Our initial investigation into transcriptome dynamics across proliferating, quiescent, and senescent primary HDFs revealed the upregulation of the hY RNA family in non-proliferating cell conditions possessing reduced translation activity (Fig. 1A and B). HDFs from two independent donors exhibited significantly increased hY RNA levels in quiescent and senescent states compared to their proliferating counterparts, a finding that was further validated via northern blot (NB) analysis (Fig. 1C). Driven by our previous findings on rancRNA-mediated translation regulation, we analyzed the rancRNA interactome of ribosomes and polysomes in these HDFs. Considering that both quiescent and senescent cells exhibit metabolic adjustments that affect translational activities, we reasoned that these HDF cells represent a good system for uncovering novel human rancRNAs [52–54]. Deep sequencing analysis of the ribosome-bound RNome revealed a marked enrichment of hY3 and hY4 compared to the other hY RNA family members (Fig. 1D). Reverse transcription quantitative polymerase chain reaction (RT-qPCR) analysis further validated the presence of hY3 in ribosome-enriched subcellular fractions, with a consistently more pronounced signal in quiescent cells, supporting a potential ribosomal interaction of hY3 and its classification as a rancRNA (Fig. 1E). As hY4 was marginally detected in ribosome-enriched fractions, our analyses primarily focused on hY3.

To further dissect the molecular functions of hY3 RNA, we investigated its interaction with ribosomes by performing polysome profiling followed by NB analysis, using the immortalized human cervical cancer cell line HeLa as a tractable model system (Fig. 1F and G). Remarkably, hY3 substantially co-migrated with ribosomal and polysomal fractions in HeLa cells, in contrast to other members of the hY RNA family. Under normal growth conditions, ∼10% of the total cellular hY3 was detected in ribosome-associated fractions. Moreover, we noticed that hY3 co-migration with ribosomal and polysomal fractions became more prominent as cell confluency increased and translational activity decreased (Supplementary Fig. S1A), resembling the increased presence observed in ribosome-enriched fractions of quiescent HDFs. This suggested that hY3 association with the ribosome may be regulated in response to a cellular need for attenuating metabolism and translational output.

To test whether co-migration in ribosome-enriched fractions derived from ribosome association, polysome profiling was performed in the presence of the Mg^{2+}-chelator EDTA. EDTA dissociates ribosomes into the two ribosomal subunits, 40S and 60S. Upon EDTA treatment, the hY3 signal in the ribosome and polysomal fractions was markedly reduced and shifted to the ribosomal subunit fractions, suggesting that it indeed interacted with ribosomes (Fig. 1H).

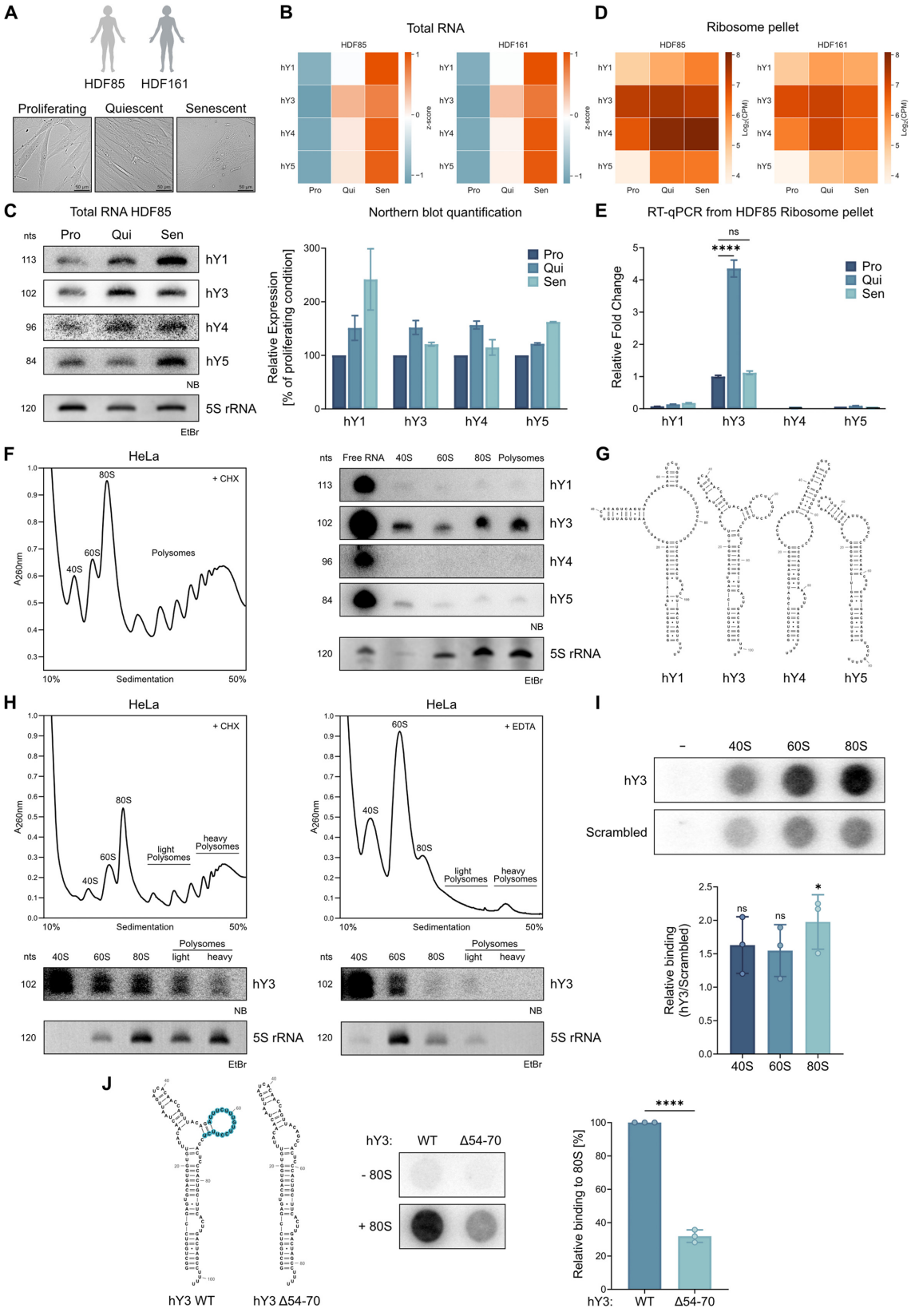

Figure 1. hY3 associates with the ribosome. (**A**) Representative microscopic images of HDFs derived from two donors (HDF85 and HDF161) which were grown in three different states: proliferating (Pro), quiescent (Qui), and doxorubicin-induced senescence (Sen). Proliferating cells, undergoing normal cell cycle progression, display a characteristic spindle-shaped morphology. Quiescent cells, growth-arrested due to contact inhibition, appear more compact. Senescent cells exhibit stable growth arrest, evident by their enlarged and flattened morphology. (**B**) Small RNA-seq analysis of total RNA from HDF cells in proliferating, quiescent, and senescent states for each donor ($n = 2$). Human Y RNA expression levels are represented as *z*-scores normalized per donor, with positive and negative values indicating relative upregulation or downregulation, respectively. (**C**) Northern blot (NB) analysis of hY RNAs using 10 μg of total RNA from proliferating, quiescent, and senescent HDF85 cells. EtBr staining of 5S rRNA is shown as loading control on an 8%

To investigate the ribosome association more directly, radiolabeled *in vitro*-transcribed hY3 was used in an *in vitro* filter binding assay utilizing purified HeLa 80S ribosomes, or isolated 40S and 60S subunits. As background binding control, a scrambled hY3 sequence was used. The binding data showed that hY3 associates only with the 80S ribosome significantly (Fig. 1I). To delineate the functional region of the hY3 molecule responsible for ribosome association, we focused on the central loop region, where variations in length and sequence are the most discriminating features among the four human Y RNAs (Fig. 1G). To test whether the loop region contributes to ribosome binding, a hY3 variant with a 17-nucleotide AU-rich deletion in the loop region was generated (Fig. 1J), a design which was inspired by a previously characterized mouse Y3 RNA mutant reported to affect translational output [21]. Filter binding assay showed that this deletion mutant (hY3 Δ54–70) displayed clearly reduced binding to the 80S ribosomes compared to the full-length hY3 (hY3 WT), implying that the deleted hY3 loop region is a determinant in ribosome binding.

Furthermore, UV crosslinking experiments were performed using radiolabeled *in vitro*-transcribed hY3, substituted with 4-thio-uridines. Following incubation with purified ribosomes and UV irradiation at 365 nm, two distinct crosslinked signals were detected by autoradiography. This crosslinking pattern differed from that of the scrambled controls (Supplementary Fig. S1B). The disappearance of the signals upon proteinase K treatment further suggested that hY3 interacts primarily with ribosomal proteins or ribosome-associated proteins rather than rRNA.

Collectively, these findings support the view that hY3 associates with human ribosomes and polysomes, mediated at least in part by its loop sequence, and suggest that hY3 represents an interesting novel rancRNA candidate worth of deeper investigation.

hY3 inhibits translation *in vitro* and in cellulo

The association of hY3 with ribosomes led us to hypothesize that it may function as a regulatory ncRNA in protein biosynthesis. To investigate whether hY3 affects translation under defined *in vitro* conditions, we employed a cell-free translation system based on crude HeLa cell lysates [43]. *De novo* protein synthesis was quantified by the incorporation of radioactive ^{35}S-methionine. Supplementation with *in vitro*-transcribed hY3 consistently reduced global translation by ∼30%. In contrast, neither a scrambled sequence, nor hY1 RNA caused a significant effect, suggesting a sequence-specific inhibitory role of hY3 in translation (Fig. 2A and B).

To corroborate the inhibitory effect of hY3 on translation observed *in vitro*, we extended our analysis to a cell-based system. We overexpressed hY3 WT in HeLa cells using its endogenous RNA polymerase III type 3 promoter (Fig. 2C). As a control, we overexpressed the ribosome binding-deficient hY3 mutant (hY3 Δ54–70) to investigate the contribution of the loop region to hY3 function. Consistent with the *in vitro* findings, overexpression of hY3 WT resulted in a significant reduction in protein biosynthesis, as assessed by ^{35}S-methionine incorporation (Fig. 2D). In contrast, overexpression of the hY3 deletion mutant (hY3 Δ54–70) did not significantly alter protein synthesis compared to HeLa cells transfected with the empty vector control. These results suggested that the hY3 ribosome association was important for the translation-regulatory activity. Notably, despite a robust increase in intracellular hY3 levels, translation was not completely suppressed. Given that endogenous hY3 is already abundant in cells, we hypothesized that this partial inhibition may reflect functional saturation which, as a consequence, limits the magnitude of the inhibitory effect upon overexpression.

To test this hypothesis, we asked whether hY3 depletion could relieve the inhibition and enhance translation. HeLa cells were transfected with an siRNA targeting the loop region of hY3. As controls, cells were transfected with either a non-targeting siRNA or a loop-targeting siRNA against hY1 (Fig. 2E and Supplementary Figs S2A and S4A, B). Remarkably, hY3 depletion resulted in a significant increase in global translation activity compared to both control conditions (Fig. 2F). This enhancement was further supported by polysome profiling, which revealed an increased polysome signal in hY3 depleted cells, indicative of raised translational

←

denaturing polyacrylamide gel. The experiment was performed in two biological replicates, with independent cell cultures. Quantification shows hY RNA expression relative to the proliferating baseline, with each hY RNA normalized independently. (**D**) Small RNA-seq analysis of the ribosome pellet from proliferating, quiescent, and senescent HDFs for each donor ($n = 2$). Y RNA expression levels are shown as $\log_2$(counts per million, cpm), with the color gradient indicating relative expression levels. (**E**) RT-qPCR analysis of hY RNAs in the ribosome pellet from proliferating, quiescent, and senescent HDF85 cells, measured in four technical replicates. 18S rRNA was used as a normalization control. Error bars represent standard deviation. Statistical differences between groups were assessed using a two-way analysis of variance (ANOVA) test. For hY3, a significant difference in relative fold change is observed between proliferating and quiescent cells (****$P < 0.0001$), while no significant difference is detected between proliferating and senescent cells (ns: not significant). (**F**) Polysome profiling of HeLa cell lysates treated with CHX using 10%–50% sucrose gradient and 20 A_{260} units of total RNA. Fractions corresponding to free RNA, 40S, 60S, 80S, and polysomes were collected and analyzed by NB to determine the fractional distribution of each hY RNA. EtBr staining of 5S rRNA on an 8% denaturing polyacrylamide gel was used as a control for rRNA distribution across the gradient. Representative data from two independent experiments are shown. (**G**) Secondary structures of the four human Y RNAs (hY1, hY3, hY4, and hY5) visualized using RNAcanvas [55]. (**H**) Polysome profiling of HeLa cell lysates treated with either CHX or the ribosome-disrupting chelating agent EDTA, using 10%–50% sucrose gradients and 10 A_{260} units of total RNA. Fractions corresponding to 40S, 60S, 80S, and light and heavy polysomes were collected and analyzed by NB to assess the distribution of hY3 RNA. EtBr staining of 5S rRNA on an 8% denaturing polyacrylamide gel was used as a control for rRNA distribution across the gradient. Representative data from three independent experiments are shown. (**I**) *In vitro* filter binding assay using 3 pmol gradient-purified 40S or 60S ribosomal subunits, and 80S ribosomes from HeLa cells, incubated with 3 pmol 5′-[^{32}P]-end-labeled *in vitro*-transcribed hY3 RNA. A synthetic scrambled version of hY3 was used to assess background binding. Signals measured in the absence of ribosomal components (−) were subtracted from all binding values. Relative binding (hY3/Scrambled) is shown as a fold change, along with standard deviation from three independent binding experiments. Statistical analysis was performed using an unpaired *t*-test, with the null hypothesis that relative binding equals unity. Among all tested conditions, 80S ribosome shows a significant relative binding (*$P < 0.05$, ns: not significant). (**J**) *In vitro* filter binding assay using 3 pmol gradient-purified 80S ribosomes from HeLa cells, incubated with 3 pmol 5′-[^{32}P]-end-labeled *in vitro*-transcribed full-length hY3 (hY3 WT) and deletion mutant (hY3 Δ54–70, deleted region depicted in blue). Signals measured in the absence of ribosomes (−) were subtracted from the corresponding binding values. Relative binding to 80S is shown, with the binding of hY3 WT set to 100%. Data represent the mean ± standard deviation from three independent experiments. Statistical analysis was performed using an unpaired *t*-test (****$P < 0.0001$).

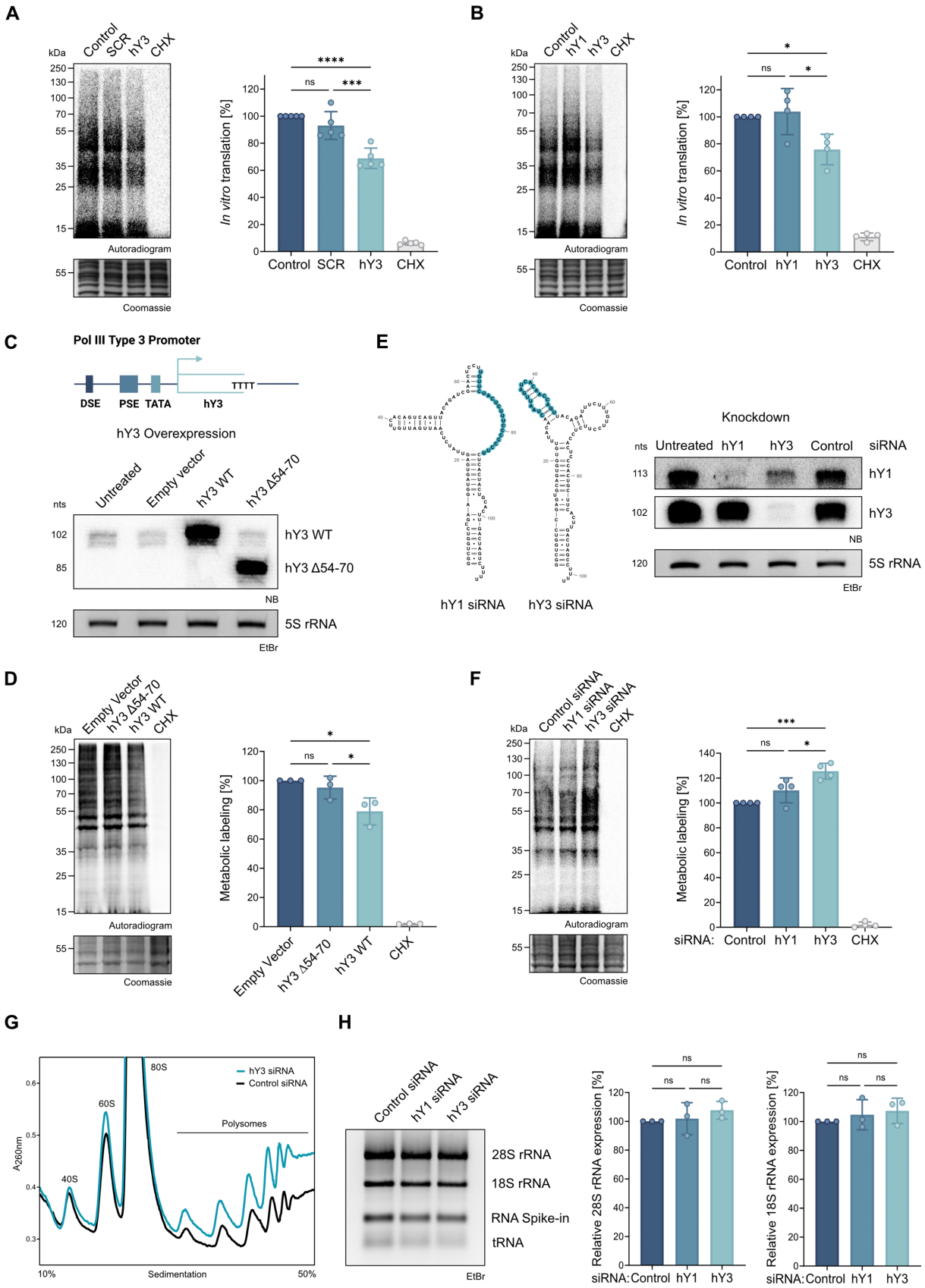

Figure 2. hY3 inhibits translation *in vitro* and *in cellulo*. (**A**) *In vitro* translation autoradiogram of dried SDS–polyacrylamide gels showing ^{35}S-radiolabeled proteins produced in the absence (Control) or presence of either 100 pmol hY3, or 100 pmol of a scrambled control RNA (SCR). Translation reactions were carried out for 20 min. Inhibition of *in vitro* protein synthesis was achieved using CHX at a final concentration of 7.5 mg/ml, confirming that the radioactive signals represented genuine *in vitro* translation products. Coomassie stained gels served as loading controls. The experiment was performed

engagement (Fig. 2G and Supplementary Fig. S2B). To determine whether this effect was due to increased ribosome content or enhanced translational efficiency, we assessed rRNA levels (Fig. 2H). hY3 knockdown led to no significant increase in fully maturated ribosomal rRNA, suggesting that changes in ribosome content are unlikely to account for the observed increase in translation.

Taken together, these results demonstrate that hY3 functions as a negative regulator of protein synthesis, both *in vitro* and *in cellulo*. Furthermore, the observation that reduction of hY3 alleviated its repressive effect on translation, combined with the high energy demand associated with translation, suggests that lower hY3 levels entail broader metabolic adaptation within cells.

hY3 impinges on the cellular metabolism

To deepen our understanding regarding the effects of hY3 depletion, we analyzed the transcriptome in HeLa cells following siRNA-mediated knockdown of hY3 by RNA-seq (Fig. 3A and Supplementary Fig. S3). Differential expression analysis identified 289 upregulated and 254 downregulated protein-coding genes (adjusted P-value < 0.05, $|\log_2 FC| > 1$) in cells with reduced hY3 levels compared to cells transfected with a non-targeting control siRNA. Functional enrichment analysis using Reactome and GO revealed an upregulation of genes associated with various metabolic processes, intracellular structures, mitochondrial function and cholesterol biosynthesis (Fig. 3B and C). These results suggested that the depletion of hY3 triggers a metabolic reprogramming shift that favors enhanced metabolic activity, energy production, and membrane synthesis.

The involvement of hY3 in the altered metabolic activities was further investigated using a Seahorse assay. Mitochondrial respiration and glycolytic activity were measured simultaneously in living HeLa cells transfected with either hY3-targeting siRNA or a non-targeting control siRNA by monitoring the OCR and ECAR, respectively (Fig. 3D and Supplementary Fig. S4C). hY3-depleted cells exhibited a higher energenic phenotype with increased mitochondrial respiration and glycolytic activity compared to control cells. To verify that this effect was indeed depending on altered hY3 levels, and not caused by putative siRNA off-targets effects, the hY3 knockdown and the seahorse assay were also performed using two other siRNA constructs targeting different regions of the hY3 (Supplementary Fig. S4A–C). The elevated mitochondrial respiration and glycolysis rates persisted also under these conditions, strongly indicating reduced hY3 levels as the cause of these effects.

This observation was further supported by a colorimetric MTT assay, which assesses mitochondrial metabolic activity through the conversion of tetrazolium salt into formazan. hY3-depleted cells showed a significant increase in metabolic activity compared with cells transfected with either a non non-targeting control siRNA or an hY1-targeting siRNA (Supplementary Fig. S4D).

To further explore this aspect, GSEA was performed on genes associated with mitochondrial function (Fig. 3E). Although the enrichment did not reach conventional thresholds for statistical significance, the results suggested a biological trend toward increased expression of mitochondrial genes following hY3 depletion.

The observed shift toward increased metabolic activity is consistent with our previous findings showing that hY3-depleted HeLa cells exhibit elevated translation rates compared with control cells (Fig. 2F and G). To further examine this relationship, gene set enrichment analyses were conducted on genes involved in cytoplasmic translation and ribosome biogenesis (Supplementary Fig. S4E). While the enrichment results for these categories did not reach statistical significance, they similarly indicated a biological trend toward enhanced translational activity upon hY3 depletion.

Concomitantly to the altered metabolism, the landscape of differential expression gene analysis revealed that hY3 depletion led to a downregulation of genes linked to extracellular matrix organization, basement membrane structure, anchoring junction, and collagen formation (Fig. 3B and C).

Together, these findings suggest that hY3 depletion promotes cellular metabolic activity at the expense of structural integrity and extracellular environment maintenance.

Depletion of hY3 results in increased translation activity and susceptibility to cell death during starvation

hY3 was more abundantly expressed in senescent and particularly in quiescent cells (Fig. 1B and C), cellular states characterized by metabolic adjustments. The observation that hY3

←

in five independent replicates ($n = 5$), including both technical and biological repeats using different HeLa cell lysate preparations. Statistical significance was determined by one-way ANOVA (***$P < 0.001$; ****$P < 0.0001$; ns, not significant). (**B**) *In vitro* translation was performed as in panel (A) with the addition of 100 pmol hY3 or hY1. The experiment was conducted in four independent replicates ($n = 4$), including both technical and biological repeats using different HeLa cell lysate preparations. Statistical significance was determined by one-way ANOVA (*$P < 0.05$). (**C**) Overexpression of hY3 WT and the hY3 deletion mutant (hY3 Δ54–70) in HeLa cells was driven by the endogenous RNA polymerase III type 3 promoter. Untreated cells and cells transfected with the empty vector served as controls. NB analysis was performed using 10 μg total RNA from transfected cells to assess hY3 expression levels. EtBr staining of 5S rRNA on an 8% denaturing polyacrylamide gel served as a loading control. (**D**) Metabolic labeling of HeLa cells overexpressing hY3 WT or the hY3 deletion mutant (hY3 Δ54–70). ^{35}S-methionine was added to the growth medium, and proteins were labeled for 1 h. The experiment was performed in three biological replicates ($n = 3$). Statistical significance was determined by one-way ANOVA (*$P < 0.05$; ns, not significant). (**E**) Knockdown of hY1 and hY3 was achieved using siRNAs targeting their respective loop regions. A non-targeting siRNA served as a control. NB analysis was performed using 20 μg total RNA from transfected cells to assess hY1 and hY3 respective expression levels. EtBr staining of 5S rRNA on an 8% denaturing polyacrylamide gel served as a loading control. (**F**) Metabolic labeling of HeLa cells with hY1 and hY3 knockdown. ^{35}S-methionine was added to the growth medium, and proteins were labeled for 1 h. CHX was added at a final concentration of 0.1 mg/ml to inhibit translation as a control. The experiment was performed in four biological replicates ($n = 4$). Statistical significance was determined by one-way ANOVA (*$P < 0.05$; ***$P < 0.001$; *ns*, not significant). (**G**) Polysome profiling of HeLa cell lysates following hY3 knockdown or transfection with control siRNA. Lysates were loaded onto 10%–50% sucrose gradients, containing 10 A_{260} units of total RNA, and centrifuged for fractionation. Representative data from two independent experiments are shown. Entire profile can be found in the supplementary (Supplementary Fig. S2B). (**H**) 28S and 18S rRNA levels were assessed in HeLa cells following hY3 and hY1 knockdown, as well as in control siRNA-transfected cells. Before RNA extraction, samples were supplemented with an RNA spike-in to serve as a normalization control. Total RNA was separated on 1% denaturing agarose gel. Statistical significance was determined by one-way ANOVA.

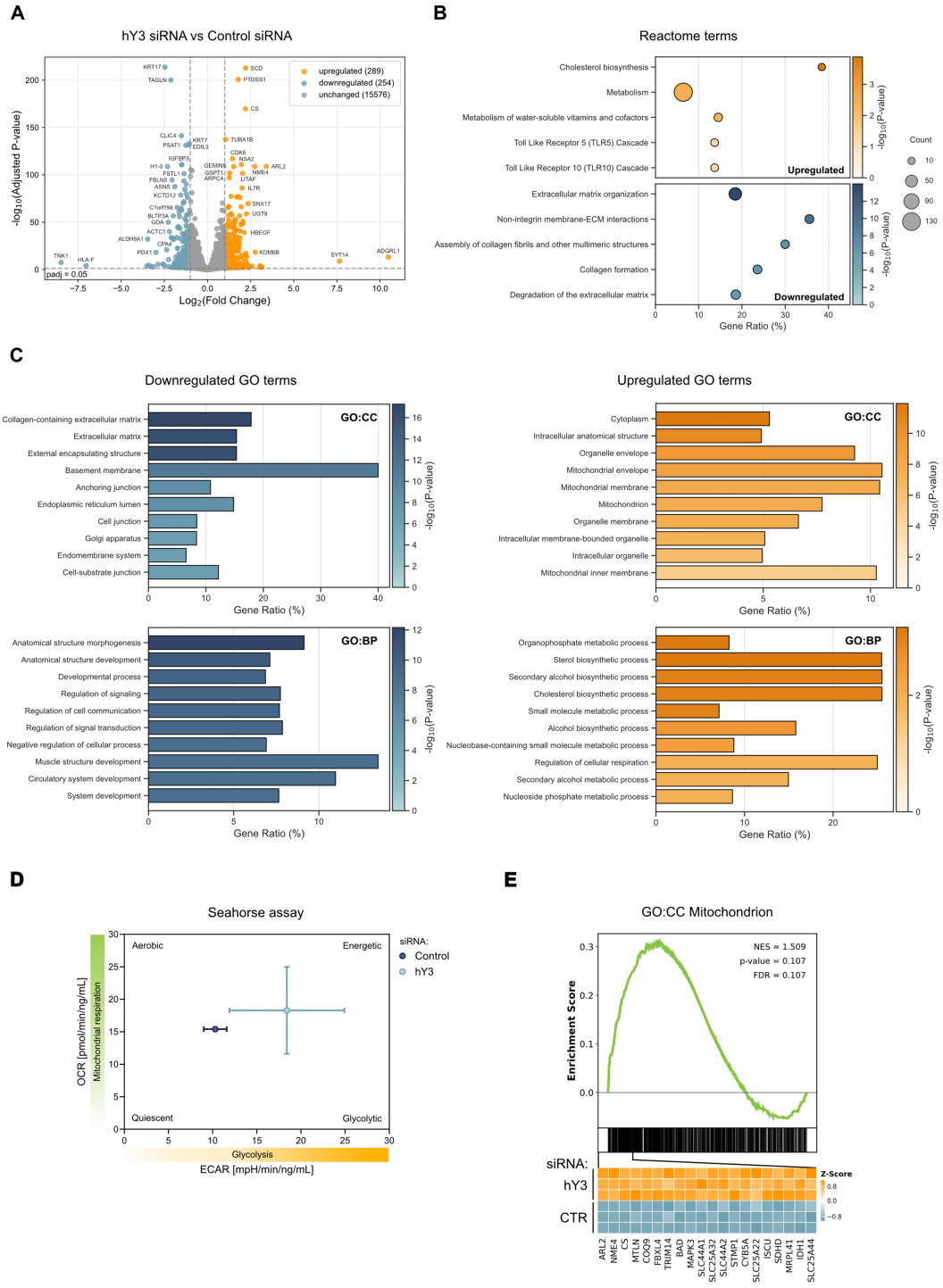

Figure 3. hY3 impinges on the cellular metabolism. (**A**) Volcano plot of differentially expressed genes in HeLa cells following siRNA-mediated knockdown of hY3, compared to cells transfected with a non-targeting control siRNA. RNA-seq was performed in biological triplicates ($n = 3$). Genes with an adjusted *P*-value < 0.05 and ± 1 $\log_2$-fold change expression are indicated by colored dots, with blue representing downregulated and orange upregulated genes. Genes are plotted according to their $\log_2$-enrichment values on the *x*-axis and adjusted *P*-values on the *y*-axis. Dashed lines indicate the enrichment and significance cutoffs. (**B**) Dot plot showing the top five significantly enriched upregulated and downregulated Reactome pathways from genes with ± 0.585 $\log_2$-fold change expression and FDR < 0.05. The *x*-axis indicates the gene ratio, the color gradient represents the enrichment *P*-value, and the size of the circles corresponds to the number of genes overlapping with each Reactome term. (**C**) Bar plots showing the top 10 significantly enriched GO terms in the categories Cellular Component (CC) and Biological Process (BP) for both upregulated and downregulated genes with ± 0.585 $\log_2$-fold change expression and FDR < 0.05. The *x*-axis represents the percentage of genes overlapping with each GO term (Gene ratio %). The color gradient reflects statistical significance, with darker colors indicating lower adjusted *P*-values. (**D**) Energy map showing the OCR, a measure of mitochondrial respiration, and the ECAR, an indicator of glycolytic activity, in living HeLa cells, as determined using a Seahorse XFe96 Analyzer. HeLa cells transfected with a non-targeting control siRNA were analyzed in two biological replicates, and hY3-depleted cells in three biological replicates; all groups included eight technical replicates. OCR and ECAR data were normalized to total DNA content and are presented as mean ± SD. (**E**) GSEA for gene sets related to Mitochondrion (GOCC_MITOCHONDRION, GO:0 005 739). Normalized enrichment score, adjusted *P*-value, and FDR are shown. The heatmap displays the top 20 leading-edge genes, scaled by *z*-score.

depletion increased metabolic activity, together with its inhibitory role in translation, led us to hypothesize that hY3 may orchestrate the cellular transition from an energetically demanding to an energy-conserving state. This shift might be facilitated by the coordinated modulation of both metabolism and protein synthesis. Such an adaptive response becomes especially important under unfavorable environmental conditions. Therefore, we reasoned that if hY3 contributes to the adaptation to limited energy resources, its absence might compromise the stress response and consequently impair the cellular ability to cope with stress.

To explore this, we investigated how hY3 influences the cellular response to nutrient starvation, a stress that conventionally requires both translational repression and metabolic downregulation. First, the distribution of hY3 in polysome profiles was examined during starvation. To this end, cells were exposed to low-glucose DMEM medium lacking amino acids and serum. Following 4 h of starvation, increased hY3 NB signals in both ribosomal and polysomal fractions were observed, suggesting enhanced association of hY3 with the ribosome (Fig. 4A). Subsequently, the functional relevance of hY3 during the early phase of nutrient deprivation was examined. For that purpose, hY3-depleted cells were exposed to 1 h of starvation. Remarkably, metabolic labeling revealed a significant increase in global translation in hY3-depleted cells, exceeding 50% (Fig. 4B and Supplementary Fig. S5A). Importantly, depletion of the hY1 paralog did not show this enhanced metabolic labeling phenotype compared with cells transfected with a non-targeting siRNA. This enhanced metabolic labeling activity again was independent on the hY3-targeting siRNA construct used (Supplementary Figs S4A and S5A). This result suggested that hY3 contributes to the prompt suppression of translation in response to nutrient shortage.

Concurrently, we observed that hY3-depleted cells were more vulnerable to prolonged starvation. During a 4-h starvation time course, cell viability was significantly reduced in hY3-depleted cells starting from 2 h onward, whereas control and hY1-depleted cells showed minimally affected survival characteristics (Fig. 4C and D; Supplementary Fig. S5B). Western blot analysis after 2 h of starvation revealed enhanced cleavage of the apoptosis marker PARP1 in hY3-depleted cells, indicating increased apoptosis (Fig. 4E). Notably, the levels of p62, an autophagy marker, decreased similarly in both hY3-depleted and control siRNA transfected cells, suggesting that autophagy, a major pro-survival response pathway to starvation, was not impaired.

These collective findings indicated that hY3's role in attenuating global translation is considerably accentuated during nutrient deprivation stress. The depletion of hY3 led to sustained translation activity under energy-limiting conditions, culminating in compromised stress adaptation and increased cell death.

Depletion of hY3 disrupts the integrated stress response and alters expression of pro-survival factors during starvation

To understand why protein synthesis remains active during starvation and to uncover the mechanisms underlying the increased susceptibility to cell death, the transcriptome and translatome changes following hY3 depletion were investigated. Given the role of hY3 as a rancRNA, a class of ncRNA known to rapidly modulate translation by directly targeting the ribosome under stress, we focused on dynamic changes during the early phase of nutrient deprivation.

To trace active translation during the first 20 min of starvation, we performed metabolic labeling by supplementing the culture medium with the methionine analog L-AHA (Fig. 5A). AHA-labeled polypeptides were then used as tags for isolating actively translating ribosomes using magnetic beads. Deep sequencing was performed of both the ribosome-captured translated mRNAs (the translatome) and total RNA from HeLa cells transfected with either hY3-targeting siRNA or a control siRNA. To specifically assess the effect of hY3 on translation, we focused on mRNAs that remained stable in expression during starvation but exhibited altered translational output (Fig. 5B). Translation efficiency analysis identified 223 significantly affected mRNAs, with 79 upregulated and 144 downregulated in hY3-depleted cells compared to the control. Notably, downregulation of the anti-apoptotic factor Bcl-xL was observed in the absence of hY3 (Fig. 5B and Supplementary Fig. S6A). Furthermore, hY3 depletion led to a decreased BCL2 expression in the transcriptome RNA-seq analysis (Fig. 5C). This negative regulation of pro-survival factors suggested a tendency toward reduced cell survival signaling, thereby inclining the cellular stress balance toward a pro-apoptotic state.

We next searched for stress-related gene expression patterns in both the transcriptome and translatome RNA-seq analysis under starvation (Fig. 5C and D; Supplementary Figs S6B and S7). Interestingly, the ASNS and the ATF4, both key components of the ISR, were significantly downregulated in hY3-depleted cells compared to controls. This implied that the absence of hY3 resulted in a compromised activation of the ISR (Fig. 5E). The ISR is a central adaptive pathway which is triggered by various stresses, including nutrient deprivation. The activation of this protective response is driven by stress-sensing kinases (PERK, GCN2, PKR, HRI), which phosphorylate eIF2α. This leads to inhibition of global protein synthesis, and concomitant promotion of selective translation of stress-responsive genes such as transcription factor ATF4. Further downstream, ASNS is transcriptionally regulated by ATF4 to support amino acid homeostasis during nutrient stress. Due to the involvement of ATF4 and ASNS in the ISR, additional ISR markers were investigated across both the transcriptome and translatome datasets [56]. And indeed, hY3 depletion resulted in a broad reduction of ISR-related gene expression at both transcriptional and translational levels (Fig. 5F). To validate these findings, we performed western blot analysis of ATF4 and ASNS under normal and starvation conditions (Fig. 5G). Upon 30 min of starvation, both ATF4 and ASNS protein level were significantly lower in hY3-depleted cells compared to controls. While starvation induced expression of ATF4 and ASNS in both hY3-depleted and control cells, the increase was significantly attenuated in hY3-depleted cells, suggesting an impairment in the activation of the ISR upstream of ATF4. To further explore this possibility, we analyzed eIF2α phosphorylation by western blot analysis. Consistent with our hypothesis, hY3-depleted cells showed reduced levels of phosphorylated eIF2α (Fig. 5G and Supplementary Fig. S8A and B), indicating insufficient global translation repression in response to starvation stress, which aligns with the earlier observation of sustained translation (Fig. 4B and Supplementary Fig. S5A). The effect of hY3 on eIF2α phosphorylation was further supported by overexpression experiments. hY3 overexpression

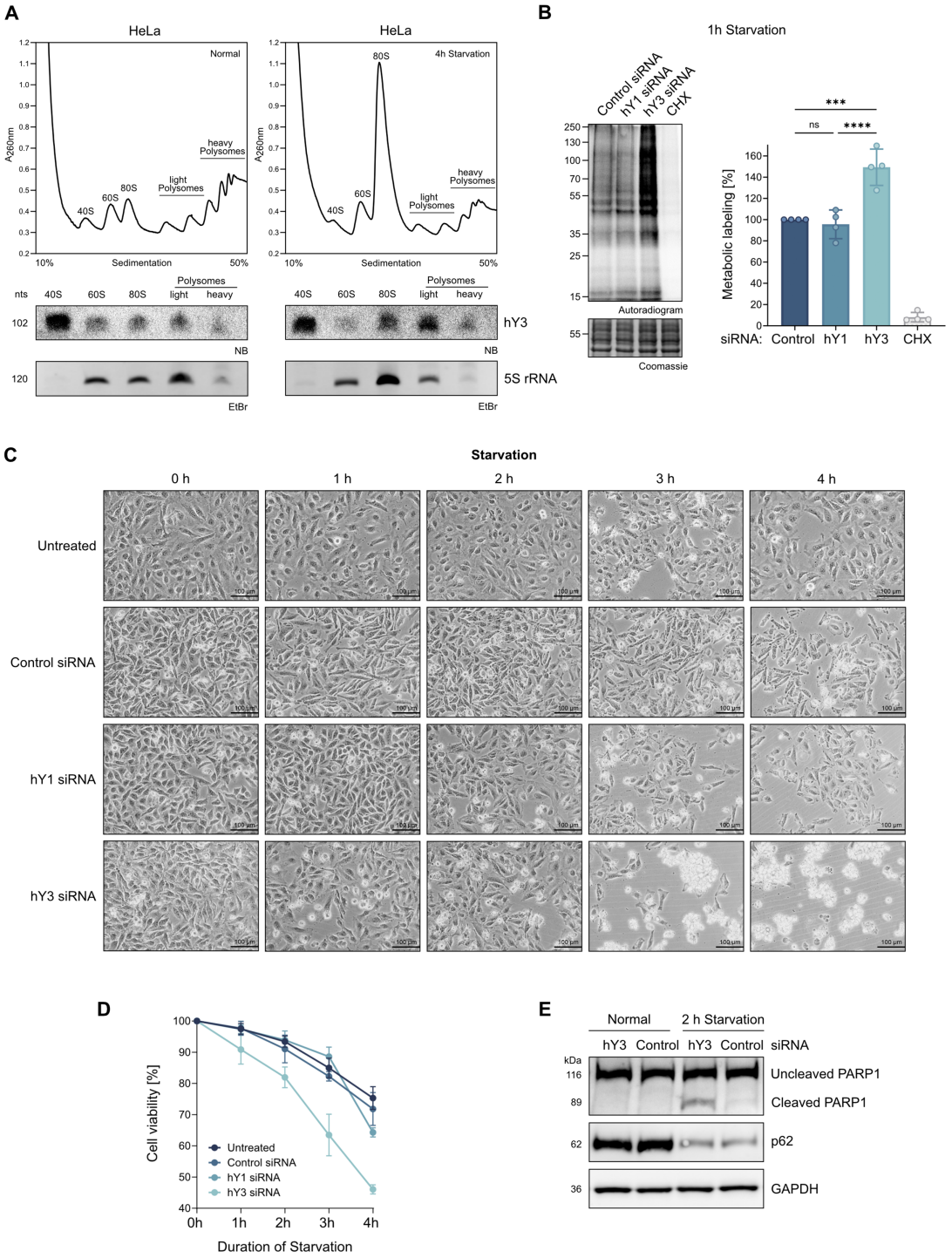

Figure 4. Depletion of hY3 results in increased translation activity and susceptibility to cell death during starvation. (**A**) Polysome profiling of HeLa cell lysates cultured under normal conditions or subjected to 4 h of starvation. Lysates containing 10 A_{260} units of total RNA were resolved on a 10%–50% sucrose gradient. Fractions corresponding to 40S, 60S, 80S ribosomal subunits, and light or heavy polysomes were collected and analyzed for hY3 by NB. EtBr staining of 5S rRNA on an 8% denaturing polyacrylamide gel served as a control for rRNA distribution across the gradient. Representative results from two independent experiments are shown. (**B**) Metabolic labeling of HeLa cells following hY1 and hY3 knockdown, or transfection with a control siRNA. Cells were incubated with ^{35}S-methionine for 1 h under starvation conditions to label newly synthesized proteins. CHX was added at a final concentration of 0.1 mg/ml to inhibit translation as a control. The experiment was performed in four biological replicates ($n = 4$), and statistical significance was assessed by one-way ANOVA (***$P < 0.001$; ****$P < 0.0001$; ns, not significant). (**C**) Representative microscopic images of untreated HeLa cells, hY1- and hY3-knockdown cells, and cells transfected with control siRNA, captured over a 4-h starvation period. For visualization, cells were grown to 100% confluency. hY3-depleted cells displayed morphological signs consistent with reduced viability under starvation stress compared with control cells. (**D**) Quantification of cell viability in untreated HeLa cells, hY1 and hY3 knockdown cells, and cells transfected with control siRNA over a 4-h starvation period. The experiment was performed in three biological replicates ($n = 3$). (**E**) Western blot analysis of hY3-knockdown and control siRNA-transfected HeLa cells cultured under normal and 2 h starvation conditions. Cleavage of the apoptosis marker PARP1 and downregulation of autophagy marker p62 following starvation were assessed. GAPDH served as a loading control. Shown are representative blots from three independent experiments.

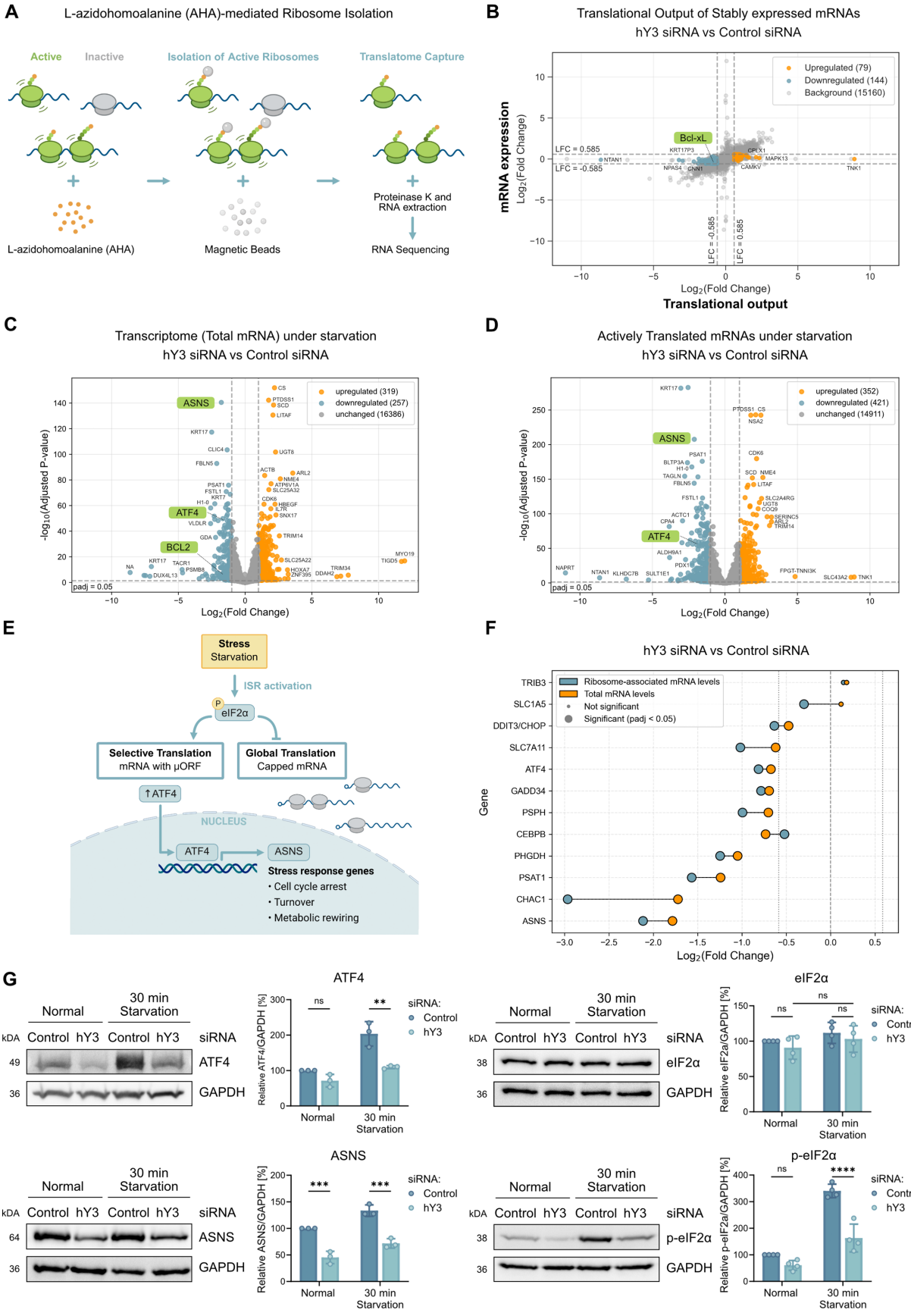

Figure 5. Depletion of hY3 disrupts the ISR and alters expression of pro survival factors during starvation. (**A**) Schematic illustrating the capture of actively translating ribosomes using the non-canonical amino acid L–AHA. Cells were subjected to 20 min of starvation in the presence of the methionine analog to label nascent peptides. AHA-labeled peptides served as affinity tags for ribosome isolation using magnetic beads. The captured

resulted in a s significant increase in phosphorylated eIF2α levels (Supplementary Fig. S8C and D). In contrast, overexpression of the ribosome binding-deficient hY3 mutant Δ54–70 did not alter p-eIF2α levels compared with cells transfected with an empty vector, highlighting the importance of hY3 ribosome-association for eIF2α phosphorylation and its role in translation regulation.

Collectively, these results demonstrated that the rancRNA hY3 plays a critical role in orchestrating the cellular stress response during starvation. Reduced hY3 levels impaired ISR activation, which resulted in incomplete translational reprogramming, followed by reduced stress adaptation, and ultimately promoting a shift toward pro-apoptotic signaling.

Discussion

The revelation of a diverse and ever-growing repertoire of ncRNAs governing fundamental cellular processes, including the fine-tuning of gene expression at both transcriptional and translational levels, is profoundly shaping our molecular understanding of cellular regulation [57, 58]. Converging evidence positions the translation machinery as a central regulatory hub modulated by ncRNAs, highlighting an emergent tier of post-transcriptional control [1].

In this study, we demonstrated that the hY3 RNA is associated with ribosomes and inhibits protein synthesis in HDF and HeLa cells (Fig. 1E, F, H, and I). hY3 is an abundant ncRNA, present at an order of magnitude of 10^5 copies in human cell [59, 60], while ∼10% thereof were found to associate to ribosomes (Fig. 1F). The ribosome-bound fraction of hY3 is likely an undeerstimatioin as the ncRNA most certainly dissociates to some extent during the polysome gradient centrifugation procedure. Furthermore, we have previously shown that targeting only a fraction of ribosomes with rancRNAs within polysomes is sufficient to yield global effects on translation [3]. Our data points to the central loop region of hY3 as a pivotal element for this ncRNA-ribosome interaction (Fig. 1J), potentially through RBP cofactors. The precise nature of this association, whether hY3 binds to the ribosome directly or through ribosome-associated proteins, remains to be clarified. Y RNAs are known for their complex interactomes, including RBPs such as Ro60 (TROVE2), La (SBB), HuR (ELAVL1), HuD (ELAVL4), polypyrimidine tract-binding protein 1 (PTBP1), HnRNP K, and IGF2BP1, all of which are involved in translational regulation and observed among ribosome-associated factors [21, 61–68]. This sustains the notion that hY3 functions as a scaffold to recruit regulatory proteins to the ribosome or as a molecular decoy [60]. Remarkably, the fact that the Y RBP Ro60 (TROVE2) has also been observed to associate with ribosomes further corroborates our finding that hY3 binds with the translation machinery [68].

Our studies showed that hY3 functions as a translational repressor *in vitro* and in a cellular context (Fig. 2A–G and Supplementary Figs S5A and S8). Increased levels of hY3 suppressed protein synthesis, while its depletion enhanced translational activity (Fig. 2D and F; Supplementary Fig. S5A). The mechanism underlying the observed translation inhibition needs yet to be clarified, namely, whether hY3 interferes with protein synthesis as a free RNA or as a part of a RNP complex that is associated with the ribosome. The role of Y3 RNA as an inhibitor of translation has previously been reported in studies conducted in mice [21]. There, mY3 has been shown to sequester HuD, and by doing so inhibit its translation enhancer activity, while the disruption of HuD-binding site within the mY3 loop region reversed this effect. This mechanism could extend to other RBPs that bind the loop region, such as the HuD paralog HuR, which has been reported to predominantly bind mY3 compared to other Y RNA family members [69]. We observed that the same deletion in the loop region of the hY3 RNA led to decreased binding efficiency to 80S ribosomes and a loss of its inhibitory effect on translation activity (Figs 1J and 2C, D; Supplementary Fig. S8C and D), supporting the functional significance of this hY3 region.

Given that protein synthesis is a highly energy-demanding process, we expected that hY3 depletion would induce a broad metabolic adaptation. Congruently, RNA-seq analysis and Seahorse assays confirmed activated metabolism upon hY3 depletion, without affecting viability under basal conditions (Fig. 3 and Supplementary Fig. S4C and D). Concomitantly,

translatome was then subjected to RNA–seq analysis. Created in BioRender. Pecoraro, V. (2026) https://BioRender.com/qzhgyys. (**B**) Scatter plot of translational output versus mRNA expression of stable mRNAs in HeLa cells under starvation following siRNA-mediated knockdown of hY3, compared with a non-targeting control siRNA. Each gene is plotted by $\log_2$-fold change in mRNA expression (*y*-axis) versus $\log_2$-fold change in translational output (*x*-axis). Stable mRNAs during starvation with an adjusted *P*-value < 0.05 are indicated with colored dots: blue for decreased and orange for increased translational output. Dashed lines denote enrichment and significance thresholds. RNAseq was performed on biological triplicates ($n = 3$). The pro-survival factor Bcl-xL is highlighted in green. (**C**) Volcano plot of differentially expressed genes in HeLa cells following siRNA-mediated knockdown of hY3, compared with a non-targeting control during 20 min of starvation. Total RNAseq was performed in biological triplicates ($n = 3$). Data are plotted as $\log_2$ enrichment (*x*-axis) versus adjusted *P*-value (*y*-axis). Genes with an adjusted *P*-value < 0.05 and ± 1 $\log_2$-fold change expression are shown as colored dots: blue for downregulated and orange for upregulated transcripts. Dashed lines indicate enrichment and significance thresholds. Genes of particular interest are highlighted in green, including ATF4, ASNS, and BCL2. (**D**) Volcano plot showing differential gene expression in ribosome-associated transcripts from HeLa cells subjected to siRNA-mediated hY3 knockdown versus non-targeting control during 20 min starvation. RNA-seq of captured translatome was conducted in biological triplicates ($n = 3$). Colored dots denote genes with adjusted *P*-value < 0.05 and ± 1 $\log_2$-fold change expression: blue for decreased and orange for increased ribosome association. Axes represent $\log_2$-enrichment (*x*-axis) and adjusted *P*-value (*y*-axis). Dashed lines mark significance and enrichment thresholds. Genes of particular interest are highlighted in green. (**E**) Schematic illustration of the ISR. Starvation-induced ISR activation triggers phosphorylation of eIF2α, resulting in global attenuation of protein synthesis with selective translation of stress-responsive mRNAs such as ATF4. ATF4 subsequently drives transcription of adaptive genes including ASNS, supporting amino acid homeostasis during nutrient shortage. Created in BioRender. Pecoraro, V. (2026) https://BioRender.com/fzfbnmk. (**F**) Comparative expression plot showing $\log_2$ fold changes in mRNA levels for a small set of ISR responsive genes [56], measured in total RNA (orange dots) and ribosome associated RNAseq (blue dots) during starvation. Dot size reflects statistical significance (*P*-value < 0.05). Dashed line indicates the ± 0.585 $\log_2$-fold change expression threshold. (**G**) Western blot analysis of ATF4, ASNS, total eIF2α, and phosphorylated eIF2α (peIF2α) was performed in HeLa cells following siRNA-mediated hY3 knockdown or non-targeting control treatment, under normal conditions or after 30 min of starvation. ATF4 and ASNS detection was performed in three biological replicates ($n = 3$), while eIF2α and p-eIF2α detection was performed in four biological replicates ($n = 4$). Statistical differences were assessed using two-way ANOVA (**$P < 0.01$; ***$P < 0.001$; ****$P < 0.0001$; *ns*: not significant).

hY3 knockdown resulted in downregulation of extracellular matrix (ECM) component genes. In support of this, previous studies have detected Y RNAs on the cell surface of HeLa cell and other mammalian cell lines, implying roles in ECM remodeling and intercellular communication [70]. Furthermore, hY3 has been described to influence the complex remodeling of the extracellular matrix by inducing a specific phenotype of cardiac fibroblasts, a process mediated through the supernatants of hY3-transfected macrophages [71].

Our findings suggest that hY3 depletion enhances cellular metabolic activity, concurrently impending cellular structural integrity and the effective maintenance of the extracellular environment (Figs 2F, 3D, and 4B; Supplementary Figs S4C and S5A). This phenotype is reminiscent of cancer cells, where enhanced energy production and elevated protein biosynthesis are prioritized over structural integrity, leading to increased invasion and metastasis potential. Consistent with these traits, reduced Y RNA levels correlate with poor prognosis and increased malignancy in human tumors [72]. The collective evidence that hY3 is found upregulated in cellular conditions of attenuated metabolism, and that its depletion leads to enhanced metabolic activity, supports the idea that this ncRNA functions as an adaptive switch, which enables the transition from an energy-consuming state to an energy-conserving one. This adaptability is particularly relevant in situations of limited energy availability, such as nutrient starvation. Interestingly, under nutrient deprivation, we observed sustained and elevated translation activity in hY3-depleted cells compared to control cells (Fig. 4B and Supplementary Fig. S5A). After 2 h of starvation, these cells appeared more susceptible to nutrient restriction, and activation of apoptosis pathway predominated, culminating after 4 h of starvation in cell death (Fig. 4C–E).

Y RNAs have previously been shown to undergo specific and rapid caspase-dependent cleavage in response to various apoptosis stimuli in different human cell lines [73]. For hY3 RNA, degradation is initiated by caspase-3-mediated truncation of its loop-binding partner, PTBP1 [74]. Notably, this process is inhibited by Bcl-2 and caspase inhibitors [73]. The cleavage of Y RNAs during apoptosis has been hypothesized to limit the exposure of the bound autoantigens such as Ro60 and La to immune surveillance, as both RNP complexes are found within apoptotic bodies at the surface of apoptotic cells [75, 76]. Reduced Y RNA cleavage during apoptosis has been associated with immune system deregulation and the onset of autoimmune diseases [74]. Interestingly, the translocation of Ro60 on the cell surface during apoptosis has been shown to depend on Y3 [77]. Furthermore, Y RNA–derived small RNAs (YsRNAs) have been reported in the context of both apoptosis and inflammation [17, 18]. Together with our observation, this suggests that full length Y3 RNAs participates in cell survival under moderate stress conditions, however, when cellular stress becomes excessive, it is actively cleaved to elicit apoptosis. In alignment with this, we observed that full-length hY3 is necessary to delay the onset of apoptosis, and its depletion affects the expression of pro-survival factors: BCL2 was downregulated at the transcriptional level, whereas Bcl-xL was downregulated at the translational level (Fig. 5B and C; Supplementary Fig. S6A). Both of these anti-apoptotic factors, on their respective regulatory levels, are controlled by the hY3-binding protein HuR [78, 79]. Together, these findings support the notion that hY3 contributes to cell survival by promoting anti-apoptotic signaling and restricting pro-apoptotic pathways.

Furthermore, our RNA-seq analysis revealed that hY3 depletion resulted in the downregulation of ISR markers, specifically ATF4 and its target ASNS (Fig. 5C, D, F, and G). The decreased levels of ATF4 and ASNS indicate that ISR activation is attenuated under stress conditions. We also investigated upstream phosphorylation of eIF2α and observed reduced phosphorylation upon hY3 depletion (Fig. 5G and Supplementary Fig. S8A and B), which may explain the sustained translation activity observed during starvation conditions. This impairment of ISR activation could lead to oxidative stress accumulation, ultimately resulting in premature cell death. eIF2α phosphorylation during starvation is mediated by the ribosome-bound GCN2 kinase [10]. Notably, the hY3-binding protein HuR has been shown to interact with GCN2 and regulate eIF2α phosphorylation, with HuR depletion leading to increased eIF2α phosphorylation [80]. In line with these previous data, our findings utilizing the ribosome-deficient hY3 variant (Fig. 2C and D; Supplementary Fig. S8C and D), which lacks the HuD/R binding site [21], suggest a functional and likely physical interaction of GCN2, HuR and hY3 on the ribosome. Thus, our data are compatible with the scenario that hY3 RNA may participate in HuR sequestration and ISR activation. The involvement of hY3 in apoptosis and ISR regulation warrants further investigation in cancer cells, which exploit the ISR to survive and regulate apoptosis [12]. Increased Y RNA have been observed in solid tumors, which are often poorly vascularized and face nutrient limitation, suggesting that hY3 could provide an adaptive advantage for cancer cells [44].

In essence, our work established hY3 RNA as a rancRNA to act on translating ribosomes as a kind of cellular “brake” that regulates metabolism and translation. It is important to note that ribosome-association is a prerequsite for affecting these activities, since a ribosome binding-deficient hY3 RNA variant (Fig. 1J) failed to modulate protein biosynthesis, eIF2α phosphorylation, and the ISR (Fig. 2D and Supplementary Fig. S8C and D). This regulatory role is crucial during stress to preserve cellular integrity, positioning hY3 as a regulatory hub at the interface of translation control and stress adaptation. Its absence leads to incomplete ISR activation, resulting in uncontrolled translation under unfavorable conditions and shifting the balance toward increased apoptosis by affecting the expression of survival determinant factors (Fig. 6). While hY3 contributes to global translation repression, it simultaneously regulates the translation of selective mRNAs, likely through its interactions with translation regulatory proteins such as HuR. Binding proteins like HuR have been shown to perform dual functions: regulating eIF2α phosphorylation, maintaining ATF4 mRNA stability, and facilitating selective translation of pro-survival factor such as Bcl-xL [79–81].

This intricate regulatory network between metabolic and survival control underscores the importance of further investigating hY3’s dynamic interactome to obtain a complete picture, which will offer valuable insights for diseases characterized by dysregulated stress responses and apoptotic signaling. To the best of our knowledge hY3 RNA represents the first characterized ncRNA that orchestrates the ISR and targets the ribosome as demonstrated here in non-proliferating HDFs and starved immortalized cancer cells.

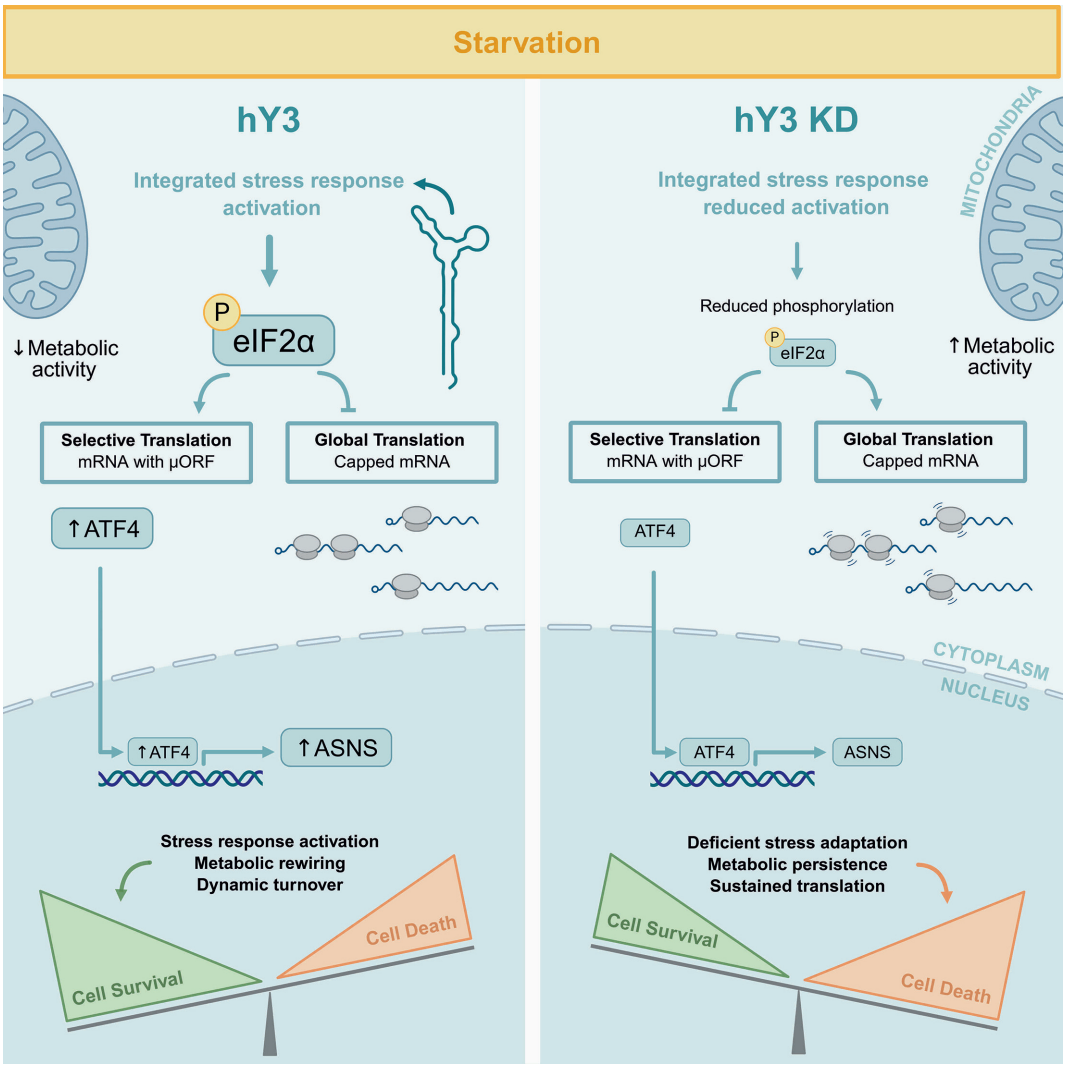

Figure 6. Model of hY3 mode of action hY3 preferentially binds to ribosomes in non-proliferating and starvation conditions and inhibits protein biosynthesis. Depletion of hY3 impairs the activation of the ISR during starvation. Reduced phosphorylation of eIF2α leads to sustained global translation and decreased selective translation of ISR-responsive transcripts such as ATF4. This in turn results in deficient induction of stress-responsive genes, including ASNS, which are necessary to restore cellular homeostasis and promote survival. As a consequence, hY3 depletion results in persistent metabolic activity under unfavorable conditions, and an incomplete adaptive response to stress, ultimately culminating in cell death. Created in BioRender. Pecoraro, V. (2026) https://BioRender.com/611igfi.

Acknowledgements

We thank Max Wolfensberger and Marc Landolfo for their experimental support. The processing of genomics data was performed on the Euler high-performance computing cluster at ETH Zürich. We thank Pamela Nicholson and her team at the next-generation sequencing (NGS) platform of the University of Bern for their valuable contributions. The graphical abstract was created in BioRender. Pecoraro, V. (2026) https://BioRender.com/ikc19uj

Author contributions: Valentina Pecoraro (Conceptualization [equal], Formal analysis [lead], Investigation [lead], Methodology [equal], Visualization [lead], Writing—original draft [lead], Writing—review & editing [equal]), Eunbin Kong (Investigation [supporting], Writing—review & editing [supporting]), Puneet Sharma (Investigation [equal], Writing—review & editing [equal]), Yulia Gonskikh (Investigation [supporting], Writing—review & editing [supporting]), Marek Zywicki (Investigation [equal], Writing—review & editing [supporting]), Fabian Nagelreiter (Investigation [supporting], Writing—review & editing [supporting]), Markus Schosserer (Resources [equal], Writing—review & editing [supporting]), Katrin Freiburghaus (Investigation [supporting], Writing—review & editing [supporting]), Jean-Marc Nuoffer (Investigation [supporting], Writing—review & editing [supporting]), Johannes Grillari (Funding acquisition [supporting], Resources [equal], Writing—review & editing [supporting]), and Norbert Polacek (Conceptualization [lead], Funding acquisition [lead], Supervision [lead], Writing—review & editing [equal]).

Supplementary data

Supplementary data is available at NAR online.

Conflict of interest

None declared.

Funding

This study was supported by the D-A-CH grant 310030E-162559/1 (to N.P.) and, in part, by 310030-188969 and 10.001.322 (to N.P.), all funded by the Swiss National Science Foundation. Additional funding came from the D-A-CH grant I2514 (to J.G.) by the Austrian Science Fund FWF. Funding to pay the Open Access publication charges for this article was provided by the Swiss National Science Foundation (10.001.322).

Data availability

High-throughput sequencing data generated in this study are deposited in the NCBI Gene Expression Omnibus (GEO) database under the accession number GSE309059 and are publicly available as of the publication date. All relevant code used for the analysis of high-throughput sequencing data is available on GitHub (https://github.com/ps-puneetsharma/pecoraro_et_al) and Zenodo (https://doi.org/10.5281/zenodo.21691269).

References

1. Pecoraro V, Rosina A, Polacek N. Ribosome-associated ncRNAs (rancRNAs) adjust translation and shape proteomes. *ncRNA* 2022;8:22. https://doi.org/10.3390/ncrna8020022
2. Pircher A, Gebetsberger J, Polacek N. Ribosome-associated ncRNAs: an emerging class of translation regulators. *RNA Biol* 2014;11:1335–9. https://doi.org/10.1080/15476286.2014.996459
3. Pircher A, Bakowska-Zywicka K, Schneider L *et al.* An mRNA-derived noncoding RNA targets and regulates the ribosome. *Mol Cell* 2014;54:147–55. https://doi.org/10.1016/j.molcel.2014.02.024
4. Reuther J, Schneider L, Iacovache I *et al.* A small ribosome-associated ncRNA globally inhibits translation by restricting ribosome dynamics. *RNA Biol* 2021;18:2617–32. https://doi.org/10.1080/15476286.2021.1935573
5. Gonskikh Y, Gerstl M, Kos M *et al.* Modulation of mammalian translation by a ribosome-associated tRNA half. *RNA Biol* 2020;17:1125–36. https://doi.org/10.1080/15476286.2020.1744296
6. Brogli R, Cristodero M, Schneider A *et al.* A ribosome-bound tRNA half stimulates mitochondrial translation during stress recovery in *Trypanosoma brucei*. *Cell Rep* 2023;42:113112. https://doi.org/10.1016/j.celrep.2023.113112
7. Sonenberg N, Hinnebusch AG. Regulation of translation initiation in eukaryotes: mechanisms and biological targets. *Cell* 2009;136:731–45. https://doi.org/10.1016/j.cell.2009.01.042
8. Biffo S, Ruggero D, Santoro MM. The crosstalk between metabolism and translation. *Cell Metab* 2024;36:1945–62. https://doi.org/10.1016/j.cmet.2024.07.022
9. Ryoo HD. The integrated stress response in metabolic adaptation. *J Biol Chem* 2024;300:107151. https://doi.org/10.1016/j.jbc.2024.107151
10. Pakos-Zebrucka K, Koryga I, Mnich K *et al.* The integrated stress response. *EMBO Rep* 2016;17:1374–95 https://doi.org/10.15252/embr.201642195
11. Balasubramanian MN, Butterworth EA, Kilberg MS. Asparagine synthetase: regulation by cell stress and involvement in tumor biology. *Am J Physiol Endo-crinol Metab* 2013;304:E789–99.
12. Tian X, Zhang S, Zhou L *et al.* Targeting the integrated stress response in cancer therapy. *Front Pharmacol* 2021;12:747837. https://doi.org/10.3389/fphar.2021.747837
13. Harding HP, Zhang Y, Zeng H *et al.* An integrated stress response regulates amino acid metabolism and resistance to oxidative stress. *Mol Cell* 2003;11:619–33. https://doi.org/10.1016/S1097-2765(03)00105-9
14. Kowalski MP, Krude T. Functional roles of non-coding Y RNAs. *Int J Biochem Cell Biol* 2015;66:20–9. https://doi.org/10.1016/j.biocel.2015.07.003
15. Zhou S, Bortle KV. The Pol III transcriptome: basic features, recurrent patterns, and emerging roles in cancer. *WIREs RNA* 2023;14:e1782. https://doi.org/10.1002/wrna.1782
16. Köhn M, Pazaitis N, Hüttelmaier S. Why Y RNAs? about versatile RNAs and their functions. *Biomolecules* 2013;3:143–56.
17. Hizir Z, Bottini S, Grandjean V *et al.* RNY (YRNA)-derived small RNAs regulate cell death and inflammation in monocytes/macrophages. *Cell Death Dis* 2017;8:e2530. https://doi.org/10.1038/cddis.2016.429
18. Shaw A, Ajit K, Chataignier M *et al.* Non-coding Y RNA fragments in a complex with YBX1 modulate PARP1 residency at DNA double strand breaks. *Nucleic Acids Research* 2025;53:gkaf517. https://doi.org/10.1093/nar/gkaf517
19. Campo A, Aliquò F, Velletri T *et al.* YRNAs: biosynthesis, structure, functions and involvment in cancer development. *Discov Onc* 2025;16:176. https://doi.org/10.1007/s12672-025-01957-x
20. Driedonks TAP, Nolte-T'Hoen ENM. Circulating Y-RNAs in extracellular vesicles and ribonucleoprotein complexes; implications for the immune system. *Front Immunol* 2019;9:3164. https://doi.org/10.3389/fimmu.2018.03164
21. Tebaldi T, Zuccotti P, Peroni D *et al.* HuD is a neural translation enhancer acting on mTORC1-responsive genes and counteracted by the Y3 small non-coding RNA. *Mol Cell* 2018;71:256–70.e10. https://doi.org/10.1016/j.molcel.2018.06.032
22. Scheckel C, Drapeau E, Frias MA *et al.* Regulatory consequences of neuronal ELAV-like protein binding to coding and non-coding RNAs in human brain. *eLife* 2016;5:e10421. https://doi.org/10.7554/eLife.10421
23. Gulìa C, Signore F, Gaffi M *et al.* Y RNA: an overview of their role as potential biomarkers and molecular targets in human cancers. *Cancers* 2020;12:1238.
24. Repetto E, Lichtenstein L, Hizir Z *et al.* RNY-derived small RNAs as a signature of coronary artery disease. *BMC Med* 2015;13:259. https://doi.org/10.1186/s12916-015-0489-y
25. Dimri GP, Lee X, Basile G *et al.* A biomarker that identifies senescent human cells in culture and in aging skin *in vivo*. *Proc Natl Acad Sci USA* 1995;92:9363–7. https://doi.org/10.1073/pnas.92.20.9363
26. Debacq-Chainiaux F, Erusalimsky JD, Campisi J *et al.* Protocols to detect senescence-associated beta-galactosidase (SA-βgal) activity, a biomarker of senescent cells in culture and *in vivo*. *Nat Protoc* 2009;4:1798–806. https://doi.org/10.1038/nprot.2009.191
27. Honda S, Morichika K, Kirino Y. Selective amplification and sequencing of cyclic phosphate–containing RNAs by the cP-RNA-seq method. *Nat Protoc* 2016;11:476–89. https://doi.org/10.1038/nprot.2016.025
28. Martin M. Cutadapt removes adapter sequences from high-throughput sequencing reads. *EMBnet j* 2011;17:10. https://doi.org/10.14806/ej.17.1.200
29. Dobin A, Davis CA, Schlesinger F *et al.* STAR: ultrafast universal RNA-seq aligner. *Bioinformatics* 2013;29:15–21. https://doi.org/10.1093/bioinformatics/bts635
30. Love MI. Huber W, Anders S. Moderated estimation of fold change and dispersion for RNA-seq data with DESeq2. *Genome Biology* 2014;15:550. https://doi.org/10.18129/B9.BIOC.DESEQ2
31. Gebetsberger J, Zywicki M, Künzi A *et al.* tRNA-derived fragments target the ribosome and function as regulatory non-coding RNA in *Haloferax volcanii*. *Archaea* 2012;2012:1–11. https://doi.org/10.1155/2012/260909
32. Christov CP, Gardiner TJ, Szüts D *et al.* Functional requirement of noncoding Y RNAs for human chromosomal DNA replication. *Mol Cell Biol* 2006;26:6993–7004. https://doi.org/10.1128/MCB.01060-06
33. Kong E, Polacek N. TRIM21 modulates stability of pro-survival non-coding RNA vtRNA1–1 in human hepatocellular carcinoma cells. *PLoS Genet* 2025;21:e1011614. https://doi.org/10.1371/journal.pgen.1011614

34. Dahn ML, Dean CA, Jo DB *et al.* Human-specific GAPDH qRT-PCR is an accurate and sensitive method of xenograft metastasis quantification. *Mol Ther Methods Clin Dev* 2021;20:398–408. https://doi.org/10.1016/j.omtm.2020.12.010
35. Vivas-García Y, Falletta P, Liebing J *et al.* Lineage-restricted regulation of SCD and fatty acid saturation by MITF controls melanoma phenotypic plasticity. *Mol Cell* 2020;77:120–37.e9. https://doi.org/10.1016/j.molcel.2019.10.014
36. Yu F, Meng Y, Wang X *et al.* Protein lactylation of citrate synthase promotes the AKI-CKD transition by activating the NLRP3 inflammasome. *Cell Rep* 2025;44:116084. https://doi.org/10.1016/j.celrep.2025.116084
37. Chen J, Ge S-J, Feng H-J *et al.* KRT17 promotes the activation of HSCs via EMT in liver fibrosis. *J Clin Transl Hepatol* 2022;10:207–18. https://doi.org/10.14218/JCTH.2021.00101
38. Feng L, Li D, Tian Y *et al.* One-step cell biomanufacturing platform: porous gelatin microcarrier beads promote human embryonic stem cell-derived midbrain dopaminergic progenitor cell differentiation in vitro and survival after transplantation *in vivo*. *Neural Regen Res* 2024;19:458–64. https://doi.org/10.4103/1673-5374.377412
39. Fan Y, Li H, Liang X *et al.* CBX3 promotes colon cancer cell proliferation by CDK6 kinase-independent function during cell cycle. *Oncotarget* 2017;8:19934–46. https://doi.org/10.18632/oncotarget.15253
40. Torrence ME, MacArthur MR, Hosios AM *et al.* The mTORC1-mediated activation of ATF4 promotes protein and glutathione synthesis downstream of growth signals. *eLife* 2021;10:e63326. https://doi.org/10.7554/eLife.63326
41. Vasudevan D, Neuman SD, Yang A *et al.* Translational induction of ATF4 during integrated stress response requires noncanonical initiation factors eIF2D and DENR. *Nat Commun* 2020;11:4677. https://doi.org/10.1038/s41467-020-18453-1
42. Gallo S, Furler M, Sigel RKO. *In vitro* transcription and purification of RNAs of different size. *Chimia* 2005;59:812. https://doi.org/10.2533/000942905777675589
43. Gonskikh Y, Pecoraro V, Polacek N. Mammalian *in vitro* translation systems. In: Matějů D, Chao JA (eds), *The Integrated Stress Response, Methods in Molecular Biology*. New York, NY: Springer US, Vol. 2428, 2022, 101–11.
44. Christov CP, Trivier E, Krude T. Noncoding human Y RNAs are overexpressed in tumours and required for cell proliferation. *Br J Cancer* 2008;98:981–8. https://doi.org/10.1038/sj.bjc.6604254
45. Meyer C, Hertig D, Arnold J *et al.* Complex I, V, and MDH2 deficient human skin fibroblasts reveal distinct metabolic signatures by ^{1}H HR-MAS NMR. *J Inher Metab Dis* 2024;47:270–9. https://doi.org/10.1002/jimd.12696
46. Dyer SC, Austine-Orimoloye O, Azov AG *et al.*Ensembl 2025. *Nucleic Acids Res* 2025;53:D948–57. https://doi.org/10.1093/nar/gkae1071
47. Patro R, Duggal G, Love MI *et al.* Salmon provides fast and bias-aware quantification of transcript expression. *Nat Methods* 2017;14:417–9. https://doi.org/10.1038/nmeth.4197
48. Wickham H, Averick M, Bryan J *et al.* Welcome to the tidyverse *JOSS*, 2019;4:1686.
49. Love MI, Soneson C, Hickey PF *et al.* Tximeta: reference sequence checksums for provenance identification in RNA-seq. *PLoS Comput Biol* 2020;16:e1007664. https://doi.org/10.1371/journal.pcbi.1007664
50. Love MI, Huber W, Anders S. Moderated estimation of fold change and dispersion for RNA-seq data with DESeq2. *Genome Biol* 2014;15:550. https://doi.org/10.1186/s13059-014-0550-8
51. Kolberg L, Raudvere U, Kuzmin I *et al.* g:Profiler—interoperable web service for functional enrichment analysis and gene identifier mapping (2023 update). *Nucleic Acids Res* 2023;51:W207–12. https://doi.org/10.1093/nar/gkad347
52. Yang G, Schmid-Siegel M, Heissenberger C *et al.* 2′ -O- ribose methylation levels of ribosomal RNA distinguish different types of growth arrest in human dermal fibroblasts. *J Cell Sci* 2024;137:jcs261930. https://doi.org/10.1242/jcs.261930
53. Payea MJ, Anerillas C, Tharakan R *et al.* Translational control during cellular senescence. *Mol Cell Biol* 2021;41:e00512–20. https://doi.org/10.1128/MCB.00512-20
54. Marescal O, Cheeseman IM. Cellular mechanisms and regulation of quiescence. *Dev Cell* 2020;55:259–71. https://doi.org/10.1016/j.devcel.2020.09.029
55. Johnson PZ, Simon AE. RNAcanvas: interactive drawing and exploration of nucleic acid structures. *Nucleic Acids Res* 2023;51:W501–8. https://doi.org/10.1093/nar/gkad302
56. Quirós PM, Prado MA, Zamboni N *et al.* Multi-omics analysis identifies ATF4 as a key regulator of the mitochondrial stress response in mammals. *J Cell Biol* 2017;216:2027–45.
57. Statello L, Guo C-J, Chen L-L *et al.* Gene regulation by long non-coding RNAs and its biological functions. *Nat Rev Mol Cell Biol* 2021;22:96–118. https://doi.org/10.1038/s41580-020-00315-9
58. Esteller M. Non-coding RNAs in human disease. *Nat Rev Genet* 2011;12:861–74. https://doi.org/10.1038/nrg3074
59. Kheir E, Krude T. Non-coding Y RNAs associate with early replicating euchromatin in concordance with the origin recognition complex. *J Cell Sci* 2017;130:1239–50. https://doi.org/10.1242/jcs.197566
60. Täuber H, Hüttelmaier S, Köhn M. POLIII-derived non-coding RNAs acting as scaffolds and decoys. *J Mol Cell Biol* 2019;11:880–5. https://doi.org/10.1093/jmcb/mjz049
61. Mishra S, Kumar A, Kumari P *et al.* Thermodynamics and binding mechanism of insulin-like growth factor binding protein 1 (IGF2BP1) and Y3 RNA interaction. *Biochemistry* 2025;64–3535–48. https://doi.org/10.1021/acs.biochem.5c00134
62. Sim S, Wolin SL. Emerging roles for the Ro 60-kDa autoantigen in noncoding RNA metabolism. *WIREs RNA* 2011;2:686–99. https://doi.org/10.1002/wrna.85
63. Pellizzoni L, Lotti F, Rutjes SA *et al.* Involvement of the *Xenopus laevis* Ro60 autoantigen in the alternative interaction of La and CNBP proteins with the 5′UTR of L4 ribosomal protein mRNA. *J Mol Biol* 1998;281:593–608. https://doi.org/10.1006/jmbi.1998.1961
64. Crosio C. La protein has a positive effect on the translation of TOP mRNAs *in vivo*. *Nucleic Acids Res* 2000;28:2927–34. https://doi.org/10.1093/nar/28.15.2927
65. Lal A, Kawai T, Yang X *et al.* Antiapoptotic function of RNA-binding protein HuR effected through prothymosin α. *EMBO J* 2005;24:1852–62. https://doi.org/10.1038/sj.emboj.7600661
66. Sawicka K, Bushell M, Spriggs KA *et al.* Polypyrimidine-tract-binding protein: a multifunctional RNA-binding protein. *Biochem Soc Trans* 2008;36:641–7. https://doi.org/10.1042/BST0360641
67. Xu Y, Wu W, Han Q *et al.* Post-translational modification control of RNA-binding protein hnRNPK function. *Open Biol* 2019;9:180239. https://doi.org/10.1098/rsob.180239
68. Erath J, Kemper D, Mugo E *et al.* A rapid, simple, and economical method for the isolation of ribosomes and translational machinery for structural and functional studies. *Nat Commun* 2025;16:7185. https://doi.org/10.1038/s41467-025-62314-8
69. Köhn M, Ihling C, Sinz A *et al.* The Y3** ncRNA promotes the 3′ end processing of histone mRNAs. *Genes Dev* 2015;29:1998–2003.
70. Flynn RA, Pedram K, Malaker SA *et al.* Small RNAs are modified with N-glycans and displayed on the surface of living cells. *Cell* 2021;184:3109–24.e22. https://doi.org/10.1016/j.cell.2021.04.023
71. Firl CEM, Halushka M, Fraser N *et al.* Contribution of S100A4-expressing fibroblasts to anti-SSA/Ro-associated atrioventricular nodal calcification and soluble S100A4 as a biomarker of clinical severity. *Front Immunol* 2023;14:1114808. https://doi.org/10.3389/fimmu.2023.1114808

72. Tolkach Y, Stahl AF, Niehoff E-M *et al.* YRNA expression predicts survival in bladder cancer patients. *BMC Cancer* 2017;17:749. https://doi.org/10.1186/s12885-017-3746-y
73. Rutjes SA, Van Der Heijden A, Van Venrooij WJ *et al.* Rapid nucleolytic degradation of the small cytoplasmic Y RNAs during apoptosis. *J Biol Chem* 1999;274:24799–807. https://doi.org/10.1074/jbc.274.35.24799
74. Kamakura T, Kameda K, Manabe M *et al.* PTBP1 protects Y RNA from cleavage leading to its apoptosis-specific degradation. *Cell Death Discov* 2024;10:322. https://doi.org/10.1038/s41420-024-02080-6
75. Casciola-Rosen LA, Anhah G, Rosen A. Autoantigens targeted in systemic lupus erythematmus are clustered in two populations of surface structures on apoptotic keratinocytes. *J Exp Med* 1994;179:1317–30.
76. Rosen A, Casciola-Rosen L. Autoantigens as substrates for apoptotic proteases: implications for the pathogenesis of systemic autoimmune disease. *Cell Death Differ* 1999;6:6–12. https://doi.org/10.1038/sj.cdd.4400460
77. Reed JH, Sim S, Wolin SL *et al.* Ro60 requires Y3 RNA for cell surface exposure and inflammation associated with cardiac manifestations of neonatal lupus. *J Immunol* 2013;191:110–6 https://doi.org/10.4049/jimmunol.1202849
78. Ishimaru D, Ramalingam S, Sengupta TK *et al.* Regulation of Bcl-2 expression by HuR in HL60 leukemia cells and A431 carcinoma cells. *Mol Cancer Res* 2009;7:1354–66. https://doi.org/10.1158/1541-7786.MCR-08-0476
79. Durie D, Hatzoglou M, Chakraborty P *et al.* HuR controls mitochondrial morphology through the regulation of Bcl_{xL} translation. *Translation* 2013;1:e23980. https://doi.org/10.4161/trla.23980
80. Kraushar ML, Thompson K, Wijeratne HRS *et al.* Temporally defined neocortical translation and polysome assembly are determined by the RNA-binding protein Hu antigen R. *Proc Natl Acad Sci USA* 2014;111:E3815–24. https://doi.org/10.1073/pnas.1408305111
81. Sanfrancesco VC, Hood DA. Acute contractile activity induces the activation of the mitochondrial integrated stress response and the transcription factor ATF4. *J Appl Physiol* 2025;138:857–71. https://doi.org/10.1152/japplphysiol.00307.2024

Received: October 19, 2025. **Revised:** June 29, 2026. **Accepted:** July 22, 2026